Article

Nonlinear Trajectory Tracking Controller for Underwater Vehicles with Shifted Center of Mass Model

Przemyslaw Herman

Institute of Automatic Control and Robotics, Poznan University of Technology, ul. Piotrowo 3a,
60-965 Poznan, Poland; przemyslaw.herman@put.poznan.pl; Tel.: +48-61-224-4500

Abstract: This paper addresses the issue of trajectory tracking control for an autonomous underwater vehicle in the presence of parameter perturbations and disturbances in three-dimensional space. The control scheme is based on a combination of the backstepping method, the adaptive integral sliding mode control scheme, and velocity transformation resulting from the decomposition of the inertia matrix, which is symmetric. In addition, adaptive laws were applied to eliminate the effects of parameter perturbations and external disturbances. The main feature of the proposed approach is that the vehicle model is not fully symmetric but contains quantities due to the shift of the center of mass. Another important feature of the control scheme is the ability to detect some of the consequences caused by reducing the vehicle model by neglecting dynamic couplings. Numerical results on the five degrees of freedom (DOF) vehicle model show the efficiency, effectiveness, and robustness of the developed controller.

Keywords: underactuated underwater vehicle; tracking control scheme; asymmetric dynamic model; velocity conversion.

1. Introduction

Researching and developing underwater vehicles has attracted the attention of many scientists and researchers. Underwater research is a major challenge because the marine environment is complex and variable; thus, autonomous underwater vehicles (AUVs) can replace humans in performing many difficult and dangerous marine operations. Among this group of vehicles, underactuated marine vehicles are of interest as they have fewer actuators than degrees of freedom. An important reason for investigating underactuated systems is that fully actuated autonomous vehicles usually generate considerable costs and may be impractical given their weight, reliability, complexity, and efficiency. Of the various tasks that can be accomplished with these systems, one is tracking the desired trajectory.

Since general vehicle models have a complex mathematical form, due to the need to take into account both nonlinearities and disturbances from the environment, e.g., [1,2], various simplifications of these models are therefore used to design simplified control schemes. These difficulties make it very common to use reduced models of marine vehicles so that control strategies are simplified.

The basic model of a marine vehicle has six DOF and includes inertial couplings. Relevant trajectory tracking schemes can be found, for example, in [3–5]. In [3], the backstepping method and Lyapunov function were used, but the simulation example included a diagonal mass matrix. The strategy in [4] was based on artificial neural networks (ANNs) with an event-triggered control approach. The control scheme in [5] consisted of the model predictive control (MPC) method and an extended active observer. It is also sometimes assumed that the mutual couplings between variables can be ignored because they have small values, making it easier to design a control system. Such a simplification leads to the users obtaining a model with six DOF but with a diagonal inertia matrix. Examples of approaches based on the above assumption are shown in [6] (backstepping, Lyapunov

function, fuzzy observer), in [7] (combination of adaptive fuzzy control with other methods), in [8] (backstepping and sliding mode control (SMC)), in [9,10] (neural network), and in [11,12] (backstepping and Lyapunov function). Making the model simpler is mathematically beneficial, but it moves the model further away from the real object. In such a situation, experimental studies on a real vehicle are convincing, e.g., [13].

Another known simplification is to reduce the vehicle model to five DOF so that it contains a diagonal mass matrix. Such a model can be found in the book by Do and Pan [1]. There are a number of trajectory tracking algorithms for a vehicle, as described. Schemes connecting ANNs to other controllers are given in [14] (with SMC), in [15] (with optimal control), in [16] (with prescribed performance), in [17] (with Lyapunov approach), and in [18] (backstepping and event-triggered approach). Other control methods for this class of models are as follows: the dynamic surface control (DSC) technique [19], the integral terminal SMC [20], a combination of a single critic network, adaptive dynamic programming (ADP), and backstepping [21], backstepping with an integral SMC scheme using bioinspired neurodynamics [22], backstepping with a Lyapunov function [23], a bioinspired model [24], backstepping, a Lyapunov function, and active disturbance rejection control (ADRC) [25], a PID regulator with SMC [26], SMC and optimal control [27], a method based on error and velocity transformation techniques enabling the design of a practical prescribed-time controller [28] and a controller that allowed the design of the desired error dynamics combining state variables in the body's fixed coordinate and world coordinate [29]. Thus, it can be seen that the five DOF model is also used in real vehicles. However, the verification problem is similar to that for control based on six DOF models, namely, if experimental tests are not feasible for any reason, then the effectiveness of the control strategy for the simplified model with five DOF should be validated in the case of a shift in the center of mass. An effort to solve this problem has just been made in this work.

This paper proposes a tracking control for a five DOF underwater vehicle model with couplings due to a shift in the center of mass. First, the symmetric inertia matrix is decomposed to obtain the diagonal form expressed in inertial quasi-velocities (IQVs). Only then is a control strategy designed that combines backstepping and SMC. Controllers that use IQVs are applicable to tracking trajectories set in three-dimensional space for marine vehicles, but only when all input signals (for fully actuated systems) are available. In contrast, for underactuated vehicles, designing control algorithms using IQVs is challenging. The novelty of the proposed approach is that, in the event of the lack of even a single input signal, control using IQVs is not comparable to algorithms for a fully forced system. An additional advantage of control algorithms using IQVs is the ability to obtain insight into vehicle dynamics when changing dynamic parameters and the desired trajectory. Such information may be useful for preparing the correct operating conditions or modifying model parameters at the initial step of vehicle design. The proposed approach has been verified on a model representation of realistic vehicle parameters via numerical simulations. It turned out to be effective in the task of trajectory tracking, confirming the usefulness of using IQVs for control purposes. The simulation tests included one vehicle and two scenarios.

The article's contributions are as follows:

(1) Obtaining a five DOF underactuated marine vehicle model with coupling by diagonalization of the inertia matrix. This model is a generalization of the usually considered models. This is an extension of commonly used control schemes for marine vehicles with a diagonal inertia matrix to an algorithm suitable for vehicles with a lack of symmetry.

(2) The design of a trajectory tracking control scheme for a vehicle moving in three-dimensional space that uses IQVs in traditional control methods. An important feature of the approach offered is the ability to examine the effect of shifting the mass center of the vehicles on the controller's performance to see some of the consequences of simplifying a model containing dynamic couplings to one that ignores those couplings.

(3) Simulation verification of the proposed strategy assuming different operating conditions regarding trajectories and couplings. A model of a real vehicle was adopted and, in contrast to some of the known work, the technical possibilities of the actuators were taken into account in order to provide operating conditions close to real ones.

It is not difficult to see that in the literature, trajectory tracking of five DOF vehicles by means of an experiment is rarely found because various problems associated with it have to be solved [29,30]. Much more often, work ends with simulation verification and the vehicle model is described by a diagonal inertia matrix. The proposed approach seems particularly useful at the design stage or in deciding whether to carry out an eventual real-world experiment because it indicates what difficulties may arise from using the controller if the center of mass is not identically located to the geometric center.

The article is organized as follows. Section 2 describes the problem under consideration. Section 3 presents the theorem concerning the proposed strategy. Section 4 contains simulation results confirming the effectiveness of the controller. Section 5 concludes the paper. The theoretical supplements can be found in Appendixes A and B.

2. Description of Problem

2.1. Underactuated Marine Vehicle Model

An underactuated marine vehicle and the frame coordinates are presented in Figure 1.
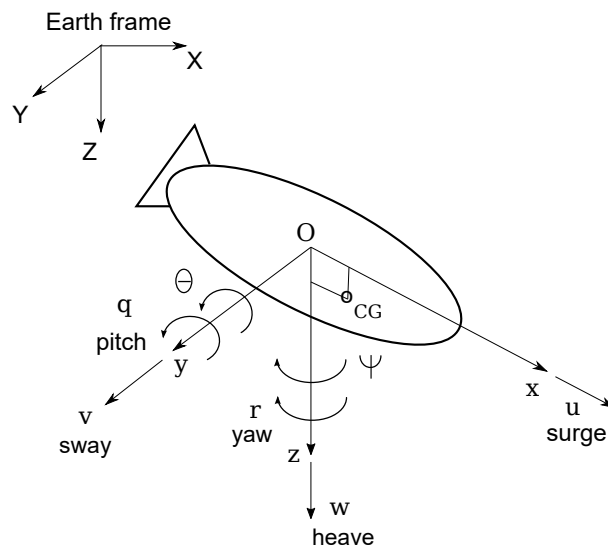

Figure 1. Underactuated underwater vehicle model and frame coordinates.

The position and orientation variables vector is $\eta = [x, y, z, \theta, \psi]^T$, whereas the kinematic and dynamic models are [2]

$$\dot{\eta} = J(\eta)\nu, \tag{1}$$

$$M\dot{\nu} + C(\nu)\nu + D(\nu)\nu + g(\eta) = \tau + \tau_D, \tag{2}$$

where $\nu = [u, v, w, q, r]^T$ means the vector of linear and angular velocities (taking into account surge, sway, heave, pitch, and yaw velocity). The vector $\tau = [\tau_u, 0, 0, \tau_q, \tau_r]^T$ means the set of control input signals. The symbol τ_D means the vector of environmental disturbances together with unknown dynamics (because, in the dynamic equation, the matrix M must be symmetric). Other matrices and vectors are ($c\theta, c\psi, s\theta, s\psi$ are abbreviations of $cos\theta, \cos\psi, \sin\theta, \sin\psi$)

$$J(\eta) = \begin{bmatrix} c\theta c\psi & -s\psi & s\theta c\psi & 0 & 0 \\ c\theta s\psi & c\psi & s\theta s\psi & 0 & 0 \\ -s\theta & 0 & c\theta & 0 & 0 \\ 0 & 0 & 0 & 1 & 0 \\ 0 & 0 & 0 & 0 & 1/c\theta \end{bmatrix}, \quad M = \begin{bmatrix} m_{11} & 0 & 0 & m_{14} & 0 \\ 0 & m_{22} & 0 & 0 & m_{25} \\ 0 & 0 & m_{33} & m_{34} & 0 \\ m_{14} & 0 & m_{34} & m_{44} & 0 \\ 0 & m_{25} & 0 & 0 & m_{55} \end{bmatrix},$$

$$C(\nu) = \begin{bmatrix} 0 & 0 & 0 & c_{14} & c_{15} \\ 0 & 0 & 0 & c_{24} & c_{25} \\ 0 & 0 & 0 & c_{34} & 0 \\ -c_{14} & -c_{24} & -c_{34} & 0 & 0 \\ -c_{15} & -c_{25} & 0 & 0 & 0 \end{bmatrix}, \quad D(\nu) = \begin{bmatrix} d_{11} & 0 & 0 & d_{14} & 0 \\ 0 & d_{22} & 0 & 0 & d_{25} \\ 0 & 0 & d_{33} & d_{34} & 0 \\ d_{41} & 0 & d_{43} & d_{44} & 0 \\ 0 & d_{52} & 0 & 0 & d_{55} \end{bmatrix}, \quad (3)$$

and $g(\eta) = [0, 0, 0, g_4, 0]^T$ (for neutrally buoyant vehicle $W = B$ with $g_4 = z_g W s\theta + x_g W c\theta$). Moreover, $J(\eta)$ denotes the transformation matrix, M denotes the mass matrix, including the added masses, $C(\nu)$ denotes the Coriolis and centripetal forces matrix, and $D(\nu)$ is the hydrodynamic damping matrix. The disturbances are included in vector $\tau_D = [\tau_{Du}, \tau_{Dv}, \tau_{Dw}, \tau_{Dq}, \tau_{Dr}]^T$. Elements of the matrices are defined in Appendix A. Noting that $C^\circ(\nu) = C(\nu)\nu$ and $D^\circ(\nu) = D(\nu)\nu$, one obtains

$$M\dot{\nu} + C^\circ(\nu) + D^\circ(\nu) + g(\eta) = \tau + \tau_D, \tag{4}$$

where $C^\circ(\nu) = [c_1^\circ, c_2^\circ, c_3^\circ, c_4^\circ, c_5^\circ]^T$ and $D^\circ(\nu) = [d_1^\circ, d_2^\circ, d_3^\circ, d_4^\circ, d_5^\circ]^T$. Equation (4) can be rewritten in more compact form:

$$M\dot{\nu} = F(\nu, \eta) + \tau + \tau_D, \tag{5}$$

where $F(\nu, \eta) = -[C^\circ(\nu) + D^\circ(\nu) + g(\eta)]$.

The paper considers the effect of the center of mass shift on the trajectory tracking task. For this reason, all disturbances due to parameter inaccuracies and environmental influences are collected in an additional component that reflects them. The inertia matrix, in contrast, includes displacements so that their effect on system dynamics during vehicle movement can be estimated.

Equation (4) represents a description of the dynamics that ensure that this condition is met. One of the possible decomposition methods used in this paper is given in [31]. The application of the equations expressed in IQVs for fully actuated marine vehicles can be found, e.g., in [32].

After decomposition of the matrix M, one obtains a diagonal matrix $\mathbb{N} = \hat{Y}^T M \hat{Y}$ ($\hat{Y}$ contains nominal parameters). This also means that $M = \hat{Y}^{-T} \mathbb{N} \hat{Y}^{-1}$ (both matrices are positive definite). All nonlinearities resulting from their omission from the real matrix Y occur in the modified perturbation function $f = \tau_D + \Delta Y$, where $f = [f_u, f_v, f_w, f_q, f_r]^T$. Furthermore, the nominal value of the matrix $\hat{\mathbb{N}}$ is $\hat{\mathbb{N}} = \hat{Y}^T \hat{M} \hat{Y}$.

The transformed equations in the place of (4) can be written as

$$\mathbb{N}\dot{\zeta} = -\hat{Y}^T[C^*(\nu) + D^*(\nu) + g(\eta)] + \hat{Y}^T\tau + \hat{Y}^T f, \tag{6}$$

$$\nu = \hat{Y}\zeta, \tag{7}$$

$$\hat{Y} = \begin{bmatrix} 1 & 0 & 0 & \hat{Y}_{14} & 0 \\ 0 & 1 & 0 & 0 & \hat{Y}_{25} \\ 0 & 0 & 1 & \hat{Y}_{34} & 0 \\ 0 & 0 & 0 & 1 & 0 \\ 0 & 0 & 0 & 0 & 1 \end{bmatrix}, \quad \mathbb{N} = \text{diag}\{\mathbb{N}_1, \mathbb{N}_2, \mathbb{N}_3, \mathbb{N}_4, \mathbb{N}_5\},$$

where $\zeta = [\zeta_1, \zeta_2, \zeta_3, \zeta_4, \zeta_5]^T$ denotes the IQV vector. The remaining quantities are as follows: $\mathbb{N}_1 = m_{11}$, $\mathbb{N}_2 = m_{22}$, $\mathbb{N}_3 = m_{33}$, $\mathbb{N}_4 = m_{44} - (m_{14}^2/m_{11}) - (m_{34}^2/m_{33})$,

$\mathbb{N}_5 = m_{55} - (m_{25}^2/m_{22})$, $\hat{Y}_{14} = -(\hat{m}_{14}/\hat{m}_{11})$, $\hat{Y}_{25} = -(\hat{m}_{25}/\hat{m}_{22})$, $\hat{Y}_{34} = -(\hat{m}_{34}/\hat{m}_{33})$.
The equations of motion replacing (6) have the form

$$\zeta_1 = u - \hat{Y}_{14}q, \quad \zeta_2 = v - \hat{Y}_{25}r, \quad \zeta_3 = w - \hat{Y}_{34}q, \quad \zeta_4 = q, \quad \zeta_5 = r, \tag{8}$$

$$\mathbb{N}_1\dot{\zeta}_1 = F_1(\zeta) + \tau_u + f_u, \tag{9}$$

$$\mathbb{N}_2\dot{\zeta}_2 = F_2(\zeta) + f_v, \tag{10}$$

$$\mathbb{N}_3\dot{\zeta}_3 = F_3(\zeta) + f_w, \tag{11}$$

$$\mathbb{N}_4\dot{\zeta}_4 = F_4(\zeta) + \tau_{\zeta_4} + f_{\zeta_4}, \tag{12}$$

$$\mathbb{N}_5\dot{\zeta}_5 = F_5(\zeta) + \tau_r + f_{\zeta_5}, \tag{13}$$

where

$$F_1(\zeta) = -m_{33}wq - m_{34}q^2 + m_{25}r^2 + m_{22}vr - d_{11}u - d_{14}q,$$

$$F_2(\zeta) = -mz_g qr - m_{11}ur - d_{22}v - d_{25}r,$$

$$F_3(\zeta) = m_{14}q^2 + m_{11}uq - d_{33}w - d_{34}q,$$

$$F_4(\zeta) = \hat{Y}_{14}F_1(\zeta) + \hat{Y}_{34}F_3(\zeta) + F_{41}(\zeta),$$

$$F_5(\zeta) = \hat{Y}_{25}F_2(\zeta) + F_{51}(\zeta),$$

$$F_{41}(\zeta) = m_{34}uq + (m_{33} - m_{11})uw + mz_g vr - m_{14}wq - d_{41}u - d_{43}w - d_{44}q - g_4,$$

$$F_{51}(\zeta) = -m_{25}ur + (m_{11} - m_{22})uv - d_{52}v - d_{55}r,$$

$$\tau_{\zeta_4} = \hat{Y}_{14}\tau_u + \tau_q, \quad f_{\zeta_4} = \hat{Y}_{14}f_u + \hat{Y}_{34}f_w + f_q, \quad f_{\zeta_5} = \hat{Y}_{25}f_v + f_r.$$

2.2. Preliminaries and Assumptions

The desired trajectory is defined as $\eta_d = [x_d, y_d, z_d]^T$ (smooth and continuous functions), whereas linear position errors are defined as $[x_e^E, y_e^E, z_e^E]^T = [x - x_d, y - y_d, z - z_d]^T$ (in the Earth frame). Moreover, the desired attitude angles are calculated from the relationship

$$\theta_d = -\arctan2\left(\frac{\dot{z}_d}{\sqrt{\dot{x}_d^2 + \dot{y}_d^2}}\right), \quad \psi_d = \arctan2\left(\frac{\dot{y}_d}{\dot{x}_d}\right). \tag{14}$$

Comment. In [22,33], the arctan function was used. Here, however, the arctan2 function was applied as it was used previously, e.g., in [7,18].

Furthermore, the coordinate transformation has the form (e.g., [22,23])

$$x_e = c\psi c\theta \, x_e^E + s\psi c\theta \, y_e^E - s\theta \, z_e^E, \tag{15}$$

$$y_e = -s\psi \, x_e^E + c\psi \, y_e^E, \tag{16}$$

$$z_e = c\psi s\theta \, x_e^E + s\psi s\theta \, y_e^E + c\theta \, z_e^E, \tag{17}$$

with x_e, y_e, z_e given in the body frame. After calculation of the time derivative using (1), one obtains (cf. [22,33])

$$\dot{x}_e = u - u_d(c\psi_e c\theta c\theta_d + s\theta s\theta_d) + ry_e - qz_e, \tag{18}$$

$$\dot{y}_e = v + u_d s\psi_e c\theta_d - r(x_e + z_e t\theta), \tag{19}$$

$$\dot{z}_e = w - u_d(c\psi_e s\theta c\theta_d - c\theta s\theta_d) + qx_e + ry_e t\theta, \tag{20}$$

$$\dot{\theta}_e = q - q_d, \tag{21}$$

$$\dot{\psi}_e = r/c\theta - r_d/c\theta_d, \tag{22}$$

where $t\theta = \tan\theta$ and $u_d = \sqrt{\dot{x}_d^2 + \dot{y}_d^2 + \dot{z}_d^2}$, $q_d = \dot{\theta}_d$, and $r_d = \dot{\psi}_d$.

Assumption 1. *The conditions specified for application of the five DOF model specified, e.g., in [30, 34] are met.*

Comment. In this work, CG lies in x–z plane, which means that $(x_g, 0, z_g)$ instead of $(x_g, 0, 0)$. This change in assumption is crucial to the proposed control algorithm.

Assumption 2. *The bounded perturbations of the model parameter are defined as $|m_{ij} - \hat{m}_{ij}| \leq \widetilde{m}_{ij}$, $|d_{ij} - \hat{d}_{ij}| \leq \widetilde{d}_{ij}$, $|\mathbb{N}_i - \hat{\mathbb{N}}_i| \leq \widetilde{N}_i$, in which $i, j = 1, \cdots, 5$. In inequalities, the symbols represent the differences between the actual and nominal values of the parameters, which must be at most equal to the expected upper limit. Furthermore, the desired trajectories can be designed as continuous and differentiable, are bounded, and can be applied to the controller.*

Comment. This type of assumption is known from, e.g., [6,35].

Assumption 3. *The functions f_u, f_v, f_w, f_q, f_r, as well as first time derivatives, are unknown but limited.*

Comment. Such an assumption appears in [6,35–37].

Assumption 4. *The lumped uncertainty is limited [35,36]. Moreover, the thrust saturation effect is not dominant or persistent; therefore, τ_u, τ_q, and τ_r are considered to be bounded.*

Assumption 5. *The approximation of the discontinuous signum function by the hyperbolic tangent function is allowed, as in, e.g., [38,39].*

2.3. Control Objective

The aim of this work is to design a proposed controller for trajectory tracking that is robust, will guarantee that the tracking error converges to a small region in finite time, and that will ensure all closed-loop signals have limited values. The controller will work effectively when Assumptions 1–5 are satisfied. Due to the assumptions made, it is designed for vehicles moving slowly (less than 1 m/s).

3. Control Scheme for Trajectory Tracking

This section shows how to design the proposed control that allows trajectory tracking in three-dimensional space. It can be given in the following theorem.

Theorem 1. *Consider the underactuated underwater vehicle described by (1) and (6)–(13). The aim of the control is the stabilization of trajectory tracking errors, i.e., $\lim_{t\to\infty} x_e = \rho_x$, $\lim_{t\to\infty} y_e = \rho_y$, $\lim_{t\to\infty} z_e = \rho_z$, $\lim_{t\to\infty} \theta_e = \rho_\theta$, and $\lim_{t\to\infty} \psi_e = \rho_\psi$, where $\rho_x, \rho_y, \rho_z, \rho_\theta, \rho_\psi$ are some constants that define the neighborhood of zero. This means that it is possible to guarantee the convergence of tracking errors to this neighborhood. Thus, if Assumptions $1 \div 5$ are met, then the signals from the controller τ_u, τ_{ζ_4} (including τ_u, τ_q), and τ_r enable the desired trajectory to be traced in three-dimensional space when parameter perturbations and external disturbances occur. The full control strategy includes the following:*

(a)   A kinematic algorithm for stabilizing kinematic errors;
(b)   A dynamic algorithm consisting of τ_u, τ_{ζ_4}, and τ_r, which will guide the vehicle to the desired trajectory and provide uniformly ultimate boundedness.

Proof of this theorem is given in Appendix B.

4. Numerical Simulations
4.1. Model of the Tested Vehicle and Assumptions

The underwater vehicle ROPOS described in [37,40] was assumed for testing. Its parameters are given in Table 1. It is a vehicle with a length, width, and height of 1.75 m,

2.6 m, and 1.45 m, respectively. The achievable velocities can be assumed to be $u_{max} = 1.25$ m/s and $v_{max} = 0.5 \div 0.6$ m/s.

Limitations on forces and torques due to propulsion forces were taken into account for the tests so as to guarantee a realistic tracking task: $|\tau_u| \leq 1400$ N, $|\tau_q| \leq 1768$, and $|\tau_r| \leq 350$ Nm .

Given a symmetric M matrix, as shown in Appendix A, the values $m_{14} = m_{41} = 226.8$ kgm and $m_{25} = m_{52} = 113.4$ kgm were assumed (for the original vehicle, they are omitted, but are needed for the simulation to assess the effect of the displacement of the center of mass). These values correspond to shifts in the center of mass of $z_g = 0.1$ m and $x_g = 0.05$ m.

Table 1. ROPOS ROV parameters [37,40].

Parameter	Value	Parameter	Value
L	1.75 m	X_u	725 Ns/m
b	2.6 m	Y_v	1240 Ns/m
h	1.45 m	Z_v	825 Ns/m
m	2268 kg	K_p	3000 Ns/m
J_x	1937 Nms^2	M_q	3000 Ns/m
J_y	2883 Nms^2	N_r	1804 Nms
J_z	2457 Nms^2	$X_{|u|u}$	1000 Ns^2/m^2
$X_{\dot{u}}$	−4380 kg	$Y_{|v|v}$	525 Ns^2/m^2
$Y_{\dot{v}}$	−9518 kg	$Z_{|w|w}$	400 Ns^2/m^2
$Z_{\dot{w}}$	−4268 kg	$K_{|p|p}$	100 Ns^2
$K_{\dot{p}}$	−5000 kgm^2	$M_{|q|q}$	100 Ns^2
$M_{\dot{q}}$	−5000 kgm^2	$N_{|r|r}$	72 Ns^2
$N_{\dot{r}}$	−5000 kgm^2		

Numerical calculations were made in the Matlab/Simulink environment assuming the duration of motion $t = 200$ s (linear), $t = 300$ s (complex), and time step size $\Delta t = 0.05$ s applying the Bogacki–Shampine (ODE3) method. The desired trajectories are taken to be

$$p_{d1} = [0.3\,t, \ 0.1\,t, \ 0.15\,t, \ \theta_{d1}, \ \psi_{d1}]^T, \tag{23}$$

$$p_{d2} = [0.5\,t + 5\sin(0.025\,t), \ -5\cos(0.025\,t), \ -0.1\,t, \ \theta_{d2}, \ \psi_{d2}]^T, \tag{24}$$

with initial points $p_{0d1} = [-4, 2, 0, 0, 0]^T$ ($\psi_{0d1} = 0$) and $p_{0d2} = [-2, 1, -0.2, 0, 0]^T$.

The following disturbance functions were selected:

$$\begin{bmatrix} f_u(t) \\ f_v(t) \\ f_w(t) \\ f_q(t) \\ f_r(t) \end{bmatrix} = \begin{bmatrix} 12 + \sin(0.05\,t) + 0.5\sin(0.02\,t) \text{ N,} \\ 1 + 0.2\sin(0.02\,t) - 0.3\cos(0.03\,t) \text{ N,} \\ 3 + 0.4\sin(0.05\,t) - 0.3\cos(0.01\,t) \text{ N} \\ 0.7 + 0.4\sin(0.01\,t) - 0.7\cos(0.05\,t) \text{ Nm} \\ 1.2 + 0.4\sin(0.03\,t) - 0.2\cos(0.02\,t) \text{ Nm} \end{bmatrix} \tag{25}$$

The designed algorithm allows for any assumptions of inaccuracy in the parameters of the dynamic model. For testing, it was assumed to be a factor of $W = 0.2$, which means a 20% parameter error.

The performance evaluation is based on the desired and realized trajectory graph and the time history of important signals and indexes.

The time history presented on graphs concern linear position errors, angular position errors, linear velocities, angular velocities, applied force and torque, kinetic energy time history, quasi-velocity errors (difference between the quasi-velocities) and velocity, i.e., $\Delta\zeta_i = \zeta_i - \nu_i$ ($i = 1, 2, 3$).

The following quantities were used to evaluate the numerical results concerning the controller performance:

(1)   Mean integrated absolute error (MIAE) for $a = x_e, y_e, z_e, \theta_e, \psi_e$;
(2)   Mean integrated absolute control (MIAC) for τ_u, τ_q, τ_r;
(3)   Root mean square of the tracking error (RMS), i.e., $RMS = \sqrt{\frac{1}{t_f - t_0} \int_{t_0}^{t_f} \|e(t)\|^2 dt}$ where

   $\|e_L(t)\| = \sqrt{(x_e)^2 + (y_e)^2 + (z_e)^2}$ (x_e, y_e, z_e mean the linear position errors in the body frame) and $\|e_A(t)\| = \sqrt{(\theta_e)^2 + (\psi_e)^2}$ (θ_e, ψ_e mean the angular position errors);
(4)   Mean kinetic energy $\text{mean}(K)$, $K = \sum_{i=1}^{3} K_i = \sum_{i=1}^{5} \frac{1}{2} N_i \zeta_i^2$ (K denotes the kinetic energy).

Controllers' parameter selection method. The selection of parameters used in the tests was based on the heuristic method described in [41], which worked well when parameters could be ranked according to their role in the controller. This intuitive method of taking into account the vehicles' dynamics can also be used for five DOF vehicles.

4.2. Algorithm Test with Weak Couplings

4.2.1. Results for Quasi-Velocity (QV) Algorithm

The following control parameters were selected for the linear trajectory:

$$k_x = 0.2, \quad k_\theta = 1.0, \quad k_\psi = 0.8, \quad \lambda_1 = \lambda_2 = \lambda_3 = 0.1, \quad \Gamma_1 = \Gamma_2 = \Gamma_3 = 0.1,$$
$$\beta_1 = 8, \quad \beta_2 = 0.2, \quad \beta_3 = 8. \tag{26}$$

Linear trajectory. The linear trajectory is tracked correctly, as can be observed in Figure 2a. Also, linear and angular errors, as shown in Figure 2b,c, decrease to their final values after about 80 s.

It is evident from Figure 2d,e that the speed u has a value that is much lower than that allowed for the ROPOS vehicle. The movement mainly takes place because of this velocity, since others have much smaller values and angular velocities have negligible values. The vehicle mainly performs forward motion, as is clear from Figure 2f, since the values of the surge force τ_u are the largest. Kinetic energy (including coupling) is primarily consumed by forward motion, as can be observed from Figure 2g. Figure 2h confirms that the dynamic couplings are very small because the linear velocity deformation values are not significant (the angular velocities are not deformed because the corresponding quasi-velocities are equal to them). For linear trajectories and weak couplings, the settling time for linear position errors is about 60 s, and for angular position errors, it is about 80 s.

Complex trajectory. The control parameters were changed due to the value of couplings, i.e.,

$$k_x = 0.2, \quad k_\theta = k_\psi = 1.0, \quad \lambda_1 = \lambda_2 = \lambda_3 = 0.1, \quad \Gamma_1 = \Gamma_2 = \Gamma_3 = 1.0,$$
$$\beta_1 = \beta_2 = \beta_3 = 0.6. \tag{27}$$

Figure 3a clearly shows that the trajectory is tracking correctly, which is also reflected by the results in Figure 3b (linear position errors). However, it is apparent from Figure 3c that the angular position errors change slightly (it is worth noting that the angular velocities are variable in character, as is evident from their calculation).
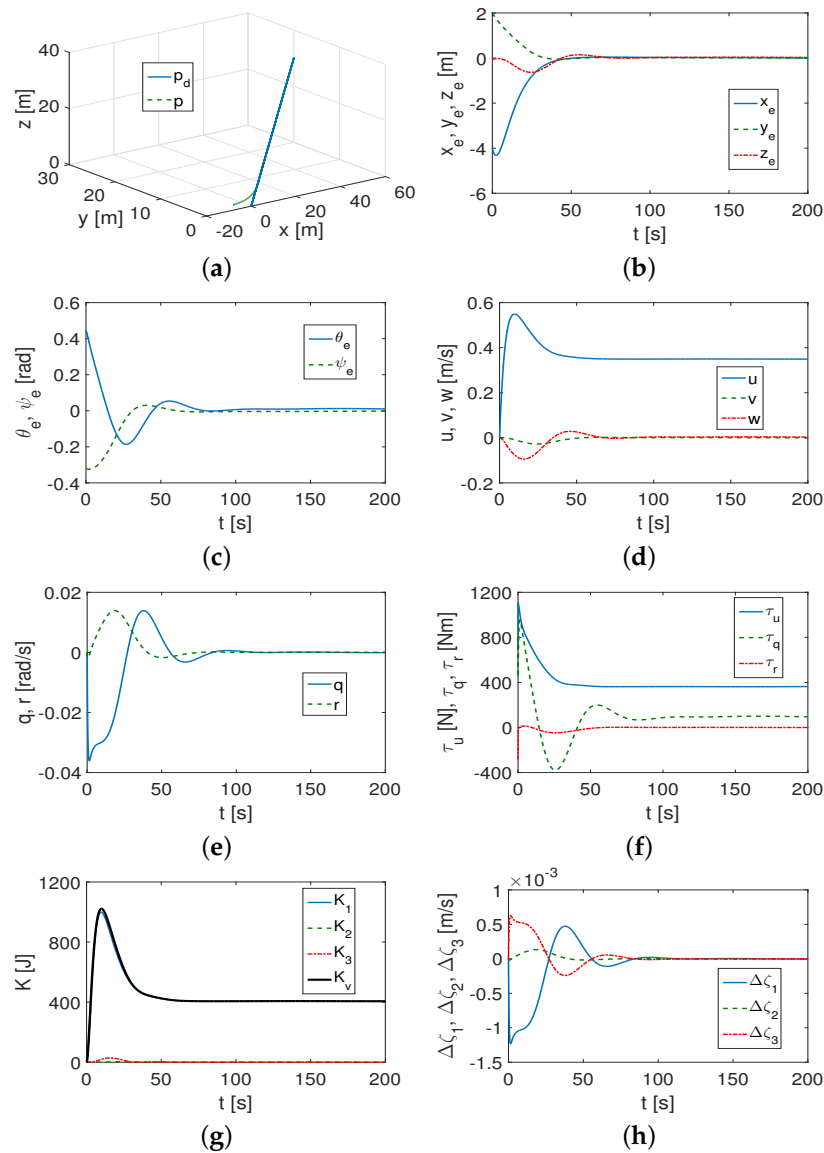
Figure 2. QV controller results, linear trajectory, and (26): (**a**) trajectories: p_d—desired, p—actual; (**b**) linear errors of position; (**c**) angular errors of position; (**d**) linear velocities; (**e**) angular velocities; (**f**) force and torque applied; (**g**) kinetic energy values; (**h**) errors of $\Delta\zeta_1, \Delta\zeta_2, \Delta\zeta_3$.

Figure 3d,e show that the linear and angular velocities are also allowed, although with slightly higher values. The movement is primarily at forward velocity u. The drive of the vehicle is mainly by means of pitch torque, and is therefore different from the linear trajectory realization. The surge force is also important, as indicated by its values in Figure 3f. However, the kinetic energy consumption is more than double that of the previous case, as illustrated in Figure 3g. It is worth noting (Figure 3h) that the deformation of linear velocities is also small, although their changes are initially oscillatory. This proves that the coupling effect value is detectable regardless of the realized trajectory. For complex trajectories and weak couplings (until a change in the direction of motion), the settling time for linear position errors is about 50 s, and for angular position errors, it is about 80 s. Thus, these times are comparable for linear and complex trajectories.
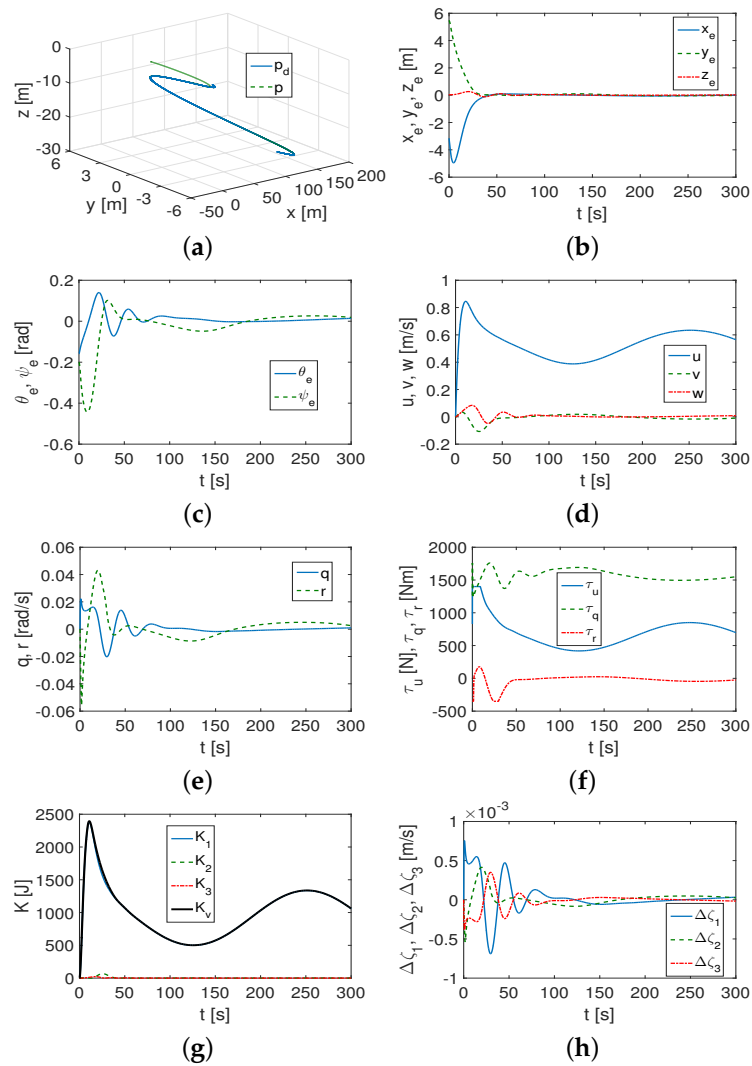
Figure 3. QV controller results, complex trajectory, and (27): (**a**) trajectories: p_d—desired, p—actual; (**b**) linear errors of position; (**c**) angular errors of position; (**d**) linear velocities; (**e**) angular velocities; (**f**) force and torque applied; (**g**) kinetic energy values; (**h**) errors of $\Delta\zeta_1, \Delta\zeta_2, \Delta\zeta_3$.

4.2.2. Results for Algorithm without Couplings

The control algorithm, which omitted couplings and was taken for comparison, was designated CL (short for classical algorithm). This control scheme is known from [22], but here the neurodynamic model is excluded, so it is closer to the concept of the same authors published in [42]. The purpose of the comparative tests is to point out differences in the performance of the control algorithm based on the inertia matrix model, which takes into account the shift of the center of mass. Since the proposed control scheme uses a combination of the backstepping technique and the adaptive integral SMC method, for comparison, a paper using the same control methods but with a diagonal inertia matrix model was selected. In this way, the effect of dynamic couplings on the controller's work and performance can be estimated. No other baseline was considered, which would have included a similar approach but with, for example, additional methods or components.

Linear trajectory. In order to show the differences in the signals obtained from the QV and CL controllers, the same set of parameters was assumed as in (26). Figure 4 demonstrates analogous results to those in Figure 2. The goal here is to make signal changes visible when the control algorithm does not take into account weak dynamic couplings resulting from small center of mass shifts. From Figure 4a, it can be observed

that not all linear positions are tracked accurately. The large tracking error z_e is due to the fact that there is no forcing signal acting on the variable z.
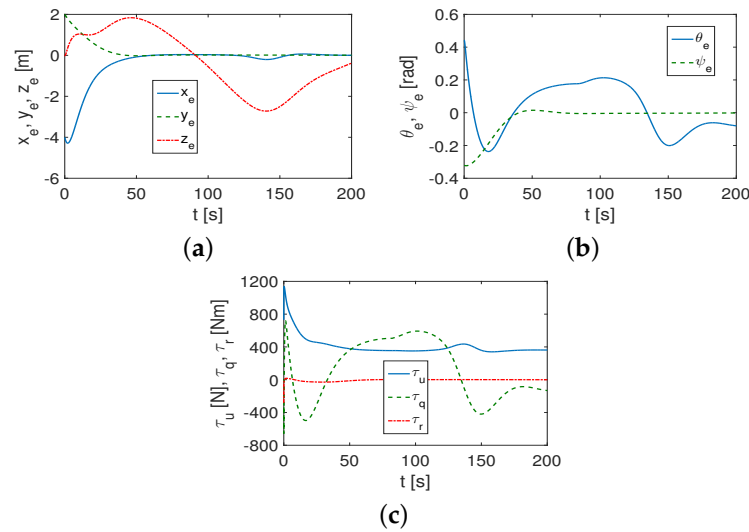

Figure 4. Comparative CL controller results, linear trajectory, and (26): (**a**) linear errors of position; (**b**) angular errors of position; (**c**) force and torque applied.

The high error values of the angular position θ_e (shown in Figure 4b) can also be explained by the lack of forcing of the variable z because the error is due to the backward and forward pitches. The results in Figure 4c show that the torque τ_q changes significantly as the vehicle moves. This proves that the controller is trying to reduce the variations caused by the dynamical couplings, but since they are constantly present, the values of this signal must also fluctuate. For linear trajectories and weak couplings, the settling time for linear position errors is about 50 s (x_e, y_e), and for angular position errors, it is about 50 s (ψ_e). The errors of the other positions do not settle, which indicates that the control algorithm is not working properly.

The aim of the next test was to obtain acceptable linear trajectory tracking. The set found was as follows:

$$k_x = 0.2, \quad k_\theta = 4.0, \quad k_\psi = 6.0, \quad \lambda_1 = 0.3, \quad \lambda_2 = \lambda_3 = 0.5, \quad \Gamma_1 = 1.0, \quad \Gamma_2 = \Gamma_3 = 0.5,$$
$$\beta_1 = 5.0, \quad \beta_2 = \beta_3 = 10. \tag{28}$$

The need to use larger gain values for the kinematic $k_\theta = 4.0, k_\psi = 6.0$, and dynamic controller $\lambda_1, \lambda_2, \lambda_3, \Gamma_1, \Gamma_2, \Gamma_3$ is due to the fact that, when using similar values to the QV scheme, similar results will not be obtained. The reason for this is that the CL controller attempts to adapt its operation to the dynamic couplings in the system. It also means that assuming even 20 percent of the unknown knowledge of the model parameters is insufficient for the CL controller to work properly.

Figure 5a shows that trajectory tracking is inaccurate and the duration of obtaining the end value increases. This is also confirmed in Figure 5b, and the reason for the inaccuracy is still the error value z_e (uncontrolled variable z). It may be observed that θ_e has a larger end error than the QV controller (Figure 5c). As is shown in Figure 5d,e, the linear velocities are similar to those of the QV controller, but the initial angular velocities have higher values. When the vehicle starts to move, the force τ_u and torque τ_q have large values, which indicates a large impulse in this phase of movement (Figure 5f).
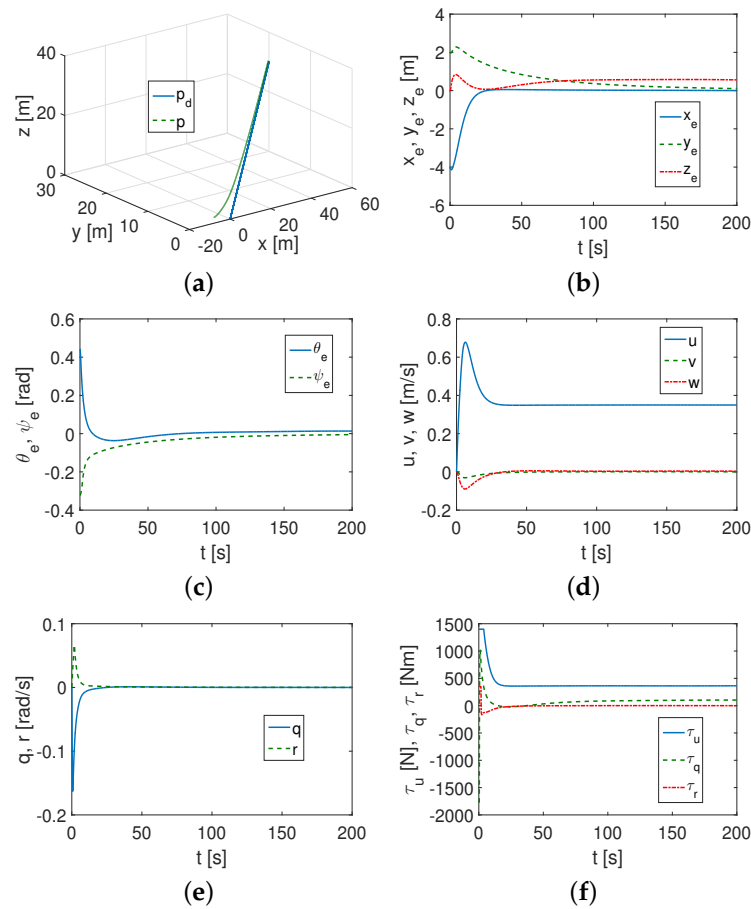
Figure 5. Comparative CL controller results, linear trajectory, and (28): (**a**) trajectories: p_d—desired, p—actual; (**b**) linear errors of position; (**c**) angular errors of position; (**d**) linear velocities; (**e**) angular velocities; (**f**) force and torque applied.

For linear trajectories, weak couplings, and new control parameters set, the settling time for linear position errors is about 200 s for y_e (and about 20 s and 80 s for x_e and z_e, respectively), and for angular position errors, it is about 80 s. The error values are higher than they are for the QV controller.

Complex trajectory. This test allowed us to check how weak dynamic couplings affect the operation of CL controller when the trajectory is changed. It turned out that the parameter set (28) also allows the tracking of a complex trajectory.

By comparing Figures 3 and 6, it can be noticed that, in the case of weak coupling, the CL algorithm is able to track the complex trajectory, but with a level of precision that may not be sufficient. Trajectory tracking is less exact than it is with the QV controller because the errors of the linear variables have larger values (cf. Figures 3a,b and 6a,b). As can be noted from Figure 6d–f, the values of speed, force, and torque show that the correct vehicle response is achieved. From a comparison of the results obtained, it is clear that the main problem is tracking linear positions when center of mass position shifts are not considered. It is worth noting, however, that it is necessary to use larger values of $\lambda_1, \lambda_2, \lambda_3$ (relating to the sliding surfaces), smaller Γ_2, Γ_3 (relating to inaccurate knowledge of the model parameters), and larger k_θ, k_ψ (relating to the kinematic controller). These modifications are due to changes in vehicle dynamics by omitting couplings.
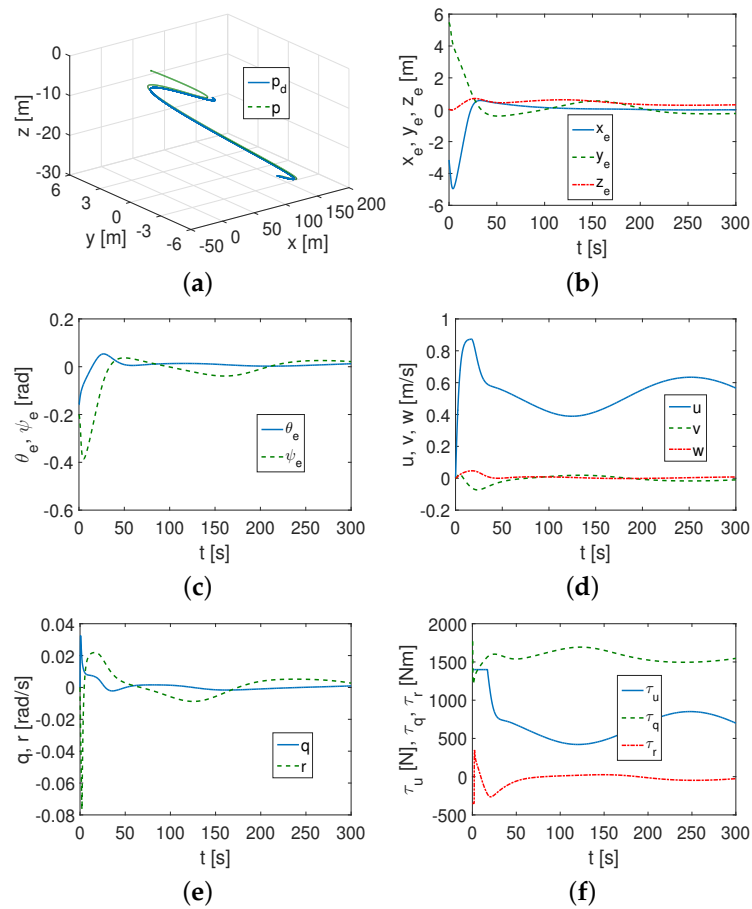
Figure 6. Comparative CL controller results and complex trajectory: (**a**) trajectories: p_d—desired, p—actual; (**b**) linear errors of position; (**c**) angular errors of position; (**d**) linear velocities; (**e**) angular velocities; (**f**) force and torque applied.

For complex trajectories, weak couplings, and new gains set (until a change in the direction of motion), the settling time for linear position errors is about 120 s, and for angular position errors, it is about 80 s. In this case, there is an improvement in the performance of the CL controller, but the linear position errors are larger than they are for the QV controller.

4.3. Algorithm Test with Stronger Couplings

This section presents the test results of the QV controller under stronger dynamic couplings than before. Shifts in the center of mass have been increased to $x_g = -0.1$ m and $z_g = 0.2$ m to show changes in the signals obtained from the system. Only the tracking of the more difficult trajectory for this task was investigated.

Complex trajectory. For the correct operation of the control scheme, the same set of parameters was sufficient, i.e., (27). From a comparison of Figures 3 and 7, little change can be observed in the signals investigated. The similarities are in Figures 3a–e,g and 7a–e,g, respectively. The τ_q signal has the opposite sign than before, although its values are comparable in both cases (Figures 3f and 7f).
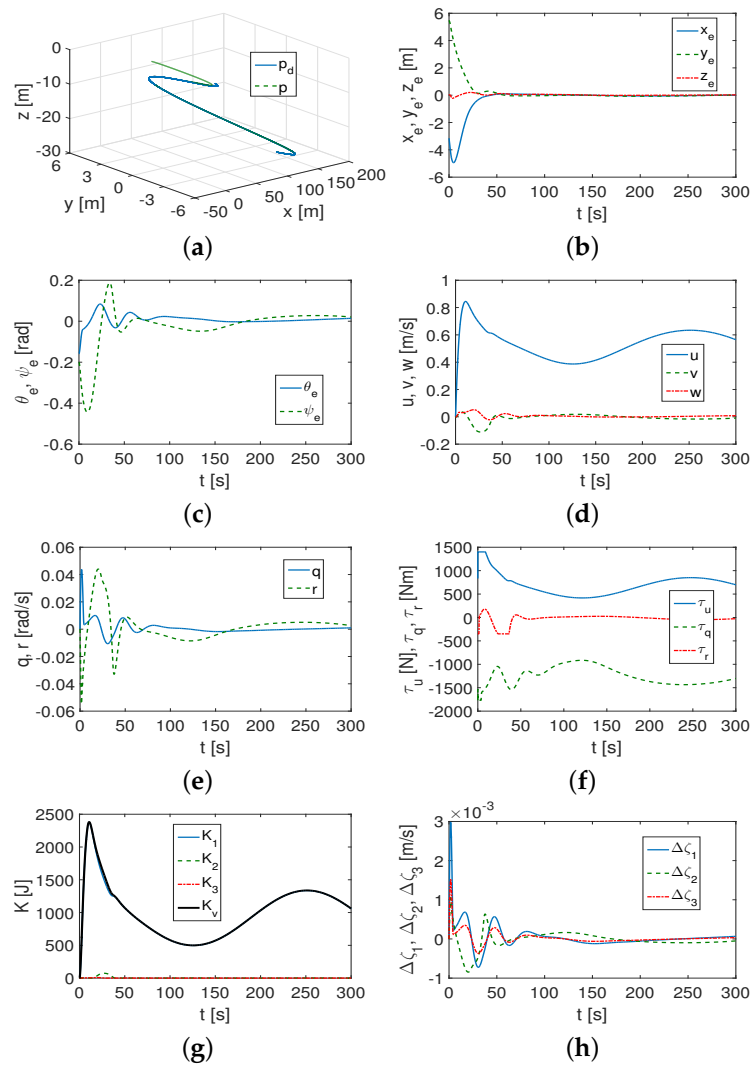
Figure 7. QV controller results, stronger couplings, complex trajectory, and (27): (**a**) trajectories: p_d—desired, p—actual; (**b**) linear errors of position; (**c**) angular errors of position; (**d**) linear velocities; (**e**) angular velocities; (**f**) force and torque applied; (**g**) kinetic energy values; (**h**) errors of $\Delta\zeta_1, \Delta\zeta_2, \Delta\zeta_3$.

It should be noted that, despite the change in the sign of x_g and the increase in z_g, the values of the control parameters may have remained the same, which may indicate their robustness to some changes in vehicle dynamics. The velocity deformations in Figures 3h and 7h clearly indicate that the coupling effects have grown (as indicated by the value of the signals at the start of the movement). For complex trajectories and strong couplings (until a change in the direction of motion), the settling time for linear position errors is about 60 s, and for angular position errors, it is about 80 s. Thus, these times are comparable for complex trajectories and weak couplings.

4.4. Results Using Indexes

The tests performed were confirmed by the results collected in Table 2.

Table 2. Performance for ROPOS

Index		QV Controller			CL Controller	
		Linear t.	Complex t.(1)	Complex t.(2)	Linear t.	Complex t.(1)
MIAE	x_e	0.3740	0.2981	0.2973	0.2026	0.3253
	y_e	0.1443	0.2393	0.2517	0.6107	0.4834
	z_e	0.1023	0.0356	0.0388	0.4713	0.4290
	θ_e	0.0436	0.0190	0.0145	0.0179	0.0134
	ψ_e	0.0351	0.0478	0.0518	0.0351	0.0423
mean	x_e	-0.3411	-0.2666	-0.2658	-0.1616	-0.1147
	y_e	0.1379	0.2134	0.1941	0.6108	0.2509
	z_e	-0.0407	0.0266	0.0276	0.4713	0.4286
	θ_e	0.0097	0.0084	0.0081	0.0052	0.0076
	ψ_e	-0.0297	-0.0221	-0.0221	-0.0351	-0.0206
std	x_e	0.9636	0.9303	0.9285	0.7007	0.9168
	y_e	0.3763	0.7915	0.7991	0.5722	0.9093
	z_e	0.1846	0.0564	0.0535	0.1706	0.1491
	θ_e	0.0854	0.0339	0.0224	0.0403	0.0205
	ψ_e	0.0828	0.0967	0.1002	0.0428	0.0808
MIAC	τ_u	403.58	699.42	699.19	401.48	700.47
	τ_q	149.48	1568.8	1249.7	87.612	1567.5
	τ_r	7.2623	47.137	50.617	11.758	48.028
RMS	$\|e_L\|$	1.1130	1.2686	1.2685	1.2109	1.3950
RMS	$\|e_A\|$	0.1229	0.1051	0.1054	0.0684	0.0861
mean	K	460.55	1019.6	1019.1	459.50	1022.9

For a linear trajectory, it is enough to compare the values of the corresponding MIAE, mean, std, and RMS. On the other hand, the values of the applied forces and torques and the kinetic energy are comparable, which indicates that the controller effort for both algorithms (QV and CL) is also comparable. If either a linear or complex (1) trajectory is tracked, smaller tracking errors y_e, z_e were obtained for the QV controller (than for CL), and therefore, in those directions for which there is no control signal. On the other hand, when there are control inputs, lower error values (x_e, θ_e, ψ_e) were obtained for the CL algorithm. The total RMS value of linear errors is lower for the QV controller, while the RMS for angular errors is lower for the CL controller. However, by comparing the time histories of these quantities (shown previously), it can be seen that the CL scheme is less effective than the QV.

For the complex trajectory in case (1), as shown in Table 2, the linear position errors (according to MIAE) are also smaller for the QV controller compared to CL, although the angular errors have slightly larger values (but not significantly). The mean values and standard deviations do not support this for x_e, but overall, the RMS confirms the higher tracking accuracy of linear variables for the QV controller. The kinetic energy consumption is slightly lower for it. There is also little difference in the average values of force and torques (MIAC index). For the complex trajectory (2), performance improvements were obtained for the QV controller. Some values of the MIAE, mean, std, MIAC, and RMS indexes were reduced. The movement took place with less control input and the kinetic energy consumption was slightly lower (it is worth noting that these increased the gains responsible for reducing the effects of inaccurately known model parameters, as for the CL controller). The omission of indexes for the CL controller in the case of the complex trajectory was due to the fact that previously worse results than those for the QV control scheme related to tracking accuracy were obtained.

It is also worth noting that although some index values are smaller for the CL controller, this does not mean that it performs better than the QV-based controller. For linear position errors, the performance of the QV controller is definitely better. On the other hand, for an-

gular position errors, the differences in numerical values are small (also their maximum values), and from the figures, it can be seen that the final values are not necessarily worse.

4.5. Analysis of Results

The control scheme was tested for a five DOF model used in ROPOS underwater vehicle marine research. The aim was to verify the effect of dynamic coupling resulting from the displacement of the center of mass relative to the geometric center. It was also taken as an assumption that verification should apply to different trajectories (linear and complex) and be performed taking into account the real technical possibilities and not only the performance of the control algorithms.

Position error convergence times of 50 to 100 s were obtained for the proposed algorithm. However, it must be taken into account that the initial position points were 2 to 6 m. Such distances, taking into account the weight of the vehicle (2268 kg) and the drag of movement in the water, significantly increase the time to reach the final positions in a steady-state motion. The convergence time depends on the initial distance points from the desired trajectory, the inertial parameters of the vehicle, and the assumed motion disturbance functions. Control algorithms for the ROPOS vehicle were tested, for example, in [37,40]. This work also took into account the limitations of the thrusters. From [37], the error convergence was achieved after about 50 s, but for an initial point less than 5 cm away from the reference trajectory. In [40], the error convergence was achieved after 25 s, but the starting distances from the desired trajectory were an order of magnitude shorter than assumed in this paper.

From the analysis of the chosen signals, the following was concluded:

1. The performance of the QV controller was correct (i.e., it ensured that the task was completed in a finite period of time) for two trajectories and for selected slow, time-varying disturbances.
2. Using the QV algorithm, it is possible to control the vehicle for both weak couplings and stronger ones resulting from the lack of full symmetry of the vehicle.
3. The simulation test based on QV provides an insight into the impact of dynamic changes in the vehicle model resulting from a shift in the center of mass and makes it possible to determine whether the control strategy in this case is effective for different trajectories.

The abovementioned observations were confirmed by an analysis of the selected indexes. This analysis shows that tracking a complex trajectory needs more kinetic energy than tracking a linear trajectory.

Remarks on the comparison of the QV algorithm with another algorithm of the same type (based on a similar control strategy and denoted as CL):

1. The QV algorithm provided acceptable performance for the assumed linear and complex trajectories, as well as for specified center-of-mass displacements.
2. This scheme can be used for comparative tests with other controls designed for trajectory tracking containing both diagonal and symmetric inertia matrix models because, after reducing the elements containing couplings, a controller for systems without couplings will be obtained. This can provide information on the effects of shifting the center of mass.
3. The QV controller allows one to determine the reduced kinetic energy of each quasi-velocity and therefore includes the coupling energy or deformation of linear velocities arising from the presence of couplings. No similar information is available with the CL controller or it will be incomplete, as in the case of kinetic energy.
4. The CL algorithm, i.e., the one in which the inertia matrix is diagonal, is able to track a complex trajectory if the dynamic couplings are weak. However, the tracking accuracy is not sufficient for the linear position. In addition, due to inaccurate information on the model parameters, higher gain values are required for the sliding surfaces and for the kinematic controller. The selection of controller parameters may not be as easy as

it is for the QV algorithm, which can be explained by the lack of inclusion of dynamic couplings in the control process.

5. The CL algorithm tested included an option for robustness to dynamic modeling errors. It was possible to obtain worse tracking errors for linear variables than for the QV scheme; therefore, the algorithm tried to overcome this problem, although with insufficient results. Without this component in the control algorithm, it would be impossible to even obtain such performance. Therefore, it is very important to take into account the possibility of changing the model parameters.

6. Using the QV algorithm, other information about changes in vehicle dynamics (velocity deformation errors) during movement can also be obtained.

5. Conclusions

The paper proposes a control scheme that is suitable for marine vehicles whose model includes dynamic couplings. The method implied transforming a model with a symmetric inertia matrix using a velocity transformation into a model where this matrix was diagonal. A control strategy consisting of two controllers, namely kinematic and dynamic, was then developed. The presented approach is particularly useful when the position of the center of mass differs from the geometric center and competing algorithms do not deliver satisfactory results. Simulation verification was carried out on a five DOF model of an ROPOS vehicle used in marine research with conditions that correspond to real operating conditions. Finally, an analysis of the results was given.

The QV control scheme made it possible to achieve acceptable performance with both weak and strong couplings for two different trajectories and under the assumption of engine limitation (according to vehicle specifications obtained from the literature). From the tests performed, it can be concluded that including the couplings arising from the shift in the center of mass in the inertia matrix is sensible because it leads to better results than when they are omitted. If the perturbation functions have small values (e.g., in the order of several N or Nm), they can represent small uncertainties in the model and environment perturbations, but inaccuracies due to a lack of symmetry should be included in the inertia matrix. Using a model with a symmetric inertia matrix resulted in better controller performance than if the model with a diagonal inertia matrix was applied.

The proposed control method is particularly useful at the pre-experimental stage (design, decision to possibly perform an experiment on a real object), as it allows the effect of dynamic couplings on the performance of the controller to be estimated.

In the future, more detailed research should point out the implications of vehicle model reduction for controller performance and include tests to determine whether the algorithm under study (known or designed) is effective when dynamic couplings are omitted from the dynamics model.

Institutional Review Board Statement: Not applicable.

Informed Consent Statement: Not applicable.

Data Availability Statement: The original contributions presented in the study are included in the article.

Conflicts of Interest: The author declares no conflicts of interest.

Appendix A

Taking into account the added mass elements of matrices,

$$m_{11} = m - X_{\dot{u}}, \quad m_{22} = m - Y_{\dot{v}}, \quad m_{33} = m - Z_{\dot{w}}, \quad m_{44} = J_y - M_{\dot{q}}, \quad m_{55} = J_z - N_{\dot{r}},$$

$$m_{14} = m_{41} = m z_g, \quad m_{25} = m_{52} = m x_g, \quad m_{34} = m_{43} = -m x_g, \tag{A1}$$

where these are the inertial elements (masses, inertias, added masses), then the elements of Coriolis terms have the form

$$
c_{14} = m_{33}w + m_{34}q, \quad c_{15} = -m_{25}r - m_{22}v, \quad c_{24} = mz_g r,
$$
$$
c_{25} = m_{11}u, \quad c_{34} = -m_{14}q - m_{11}u. \tag{A2}
$$

The hydrodynamics damping coefficients are assumed to be

$$
\begin{aligned}
&d_{11} = X_u + X_{|u|u}|u|, \quad d_{14} = X_q + X_{|q|q}|q|, \quad d_{22} = Y_v + Y_{|v|v}|v|, \quad d_{25} = Y_r + Y_{|r|r}|r| \\
&d_{33} = Z_w + Z_{|w|w}|w|, \quad d_{34} = Z_q + Z_{|q|q}|q|, \quad d_{41} = M_u + M_{|u|u}|u|, \quad d_{43} = M_w + M_{|w|w}|w|, \\
&d_{44} = M_q + M_{|q|q}|q|, \quad d_{52} = N_v + N_{|v|v}|v|, \quad d_{55} = N_r + N_{|r|r}|r|.
\end{aligned} \tag{A3}
$$

In Equation (4), the terms are

$$
\begin{aligned}
c_1^\circ &= c_{14}q + c_{15}r = m_{33}wq + m_{34}q^2 - m_{25}r^2 - m_{22}vr, \\
c_2^\circ &= c_{24}q + c_{25}r = mz_g qr + m_{11}ur, \quad c_3^* = c_{34}q = -m_{14}q^2 - m_{11}uq, \\
c_4^\circ &= c_{41}u + c_{42}v + c_{43}w = -m_{34}uq - m_{33}uw - mz_g vr + m_{14}wq + m_{11}uw, \\
c_5^* &= c_{51}u + c_{52}v = m_{25}ur + m_{22}uv - m_{11}uv.
\end{aligned} \tag{A4}
$$

whereas

$$
\begin{aligned}
d_1^\circ &= d_{11}u + d_{14}q, \quad d_2^\circ = d_{22}v + d_{25}r, \quad d_3^\circ = d_{33}w + d_{34}q, \\
d_4^\circ &= d_{41}u + d_{43}w + d_{44}q, \quad d_5^\circ = d_{52}v + d_{55}r.
\end{aligned} \tag{A5}
$$

Appendix B

In this appendix, the controllers and proof of Theorem 1 are presented.

Kinematic controller design. The Lyapunov function candidate (LFC) is assumed according the idea [43] that was presented in [22],

$$
V_K = \frac{1}{2}x_e^2 + \frac{1}{2}y_e^2 + \frac{1}{2}z_e^2 + (1 - c\theta_e) + (1 - c\psi_e), \tag{A6}
$$

in order to design the kinematic control algorithm. Calculating the time derivative of (A6) one obtains

$$
\dot{V}_K = x_e\dot{x}_e + y_e\dot{y}_e + z_e\dot{z}_e + \dot{\theta}_e s\theta_e + \dot{\psi}_e s\psi_e. \tag{A7}
$$

Applying Equations (18)–(22), grouping the terms, and denoting $s\theta_e = s(\theta - \theta_d)$, this time derivative can be given as follows:

$$
\begin{aligned}
\dot{V}_K = &\, x_e\big(u - u_d(c\psi_e c\theta c\theta_d + s\theta s\theta_d)\big) + vy_e + z_e\big(w + u_d(1 - c\psi_e)c\theta s\theta_d\big) \\
&+ (q - q_d - u_d z_e c\psi_e)s\theta_e + (r/c\theta - r_d/c\theta_d + u_d y_e c\theta_d)s\psi_e.
\end{aligned} \tag{A8}
$$

To satisfy the condition that $\dot{V}_K < 0$, the speeds u, q, r are defined as virtual control inputs. In turn, the desired velocities are assumed in the form [22]

$$
\mu_{du} = u_d(c\psi_e c\theta c\theta_d + s\theta s\theta_d) - k_x x_e, \tag{A9}
$$
$$
\mu_{dq} = q_d + u_d z_e c\psi_e - k_\theta s\theta_e, \tag{A10}
$$
$$
\mu_{dr} = (r_d/c\theta_d - u_d y_e c\theta_d - k_\psi s\psi_e)c\theta, \tag{A11}
$$

where $k_x > 0$, $k_\theta > 0$, $k_\psi > 0$ are some positive numbers. If the virtual speeds u, q, r are equivalent to the corresponding desired speeds, then applying the Equations (A9)–(A11) into (A8) one has

$$\dot{V}_K = -k_x x_e^2 - k_\theta s^2 \theta_e - k_\psi s^2 \psi_e + v y_e + z_e \left(w + u_d (1 - c\psi_e) c\theta s\theta_d \right). \tag{A12}$$

Because for any cosine function $|\cos(\cdot)| \leq 1$, thus $z_e \left(w + u_d(1 - c\psi_e)c\theta s\theta_d \right) \leq |z_e(w + 2u_d)| \leq |z_e w| + 2|z_e u_d|$. This implies that

$$\dot{V}_K \leq -k_x x_e^2 - k_\theta s^2 \theta_e - k_\psi s^2 \psi_e + |v y_e| + |z_e w| + 2|z_e u_d|. \tag{A13}$$

As direct control in the directions of movement are not guaranteed, the two lemmas are proposed. These are analogous but not the same as the lemma in [22].

Lemma A1 (based on [44]). *Assuming a limited disturbance function f_v, it is possible to limit the speed of v, which makes the rate of ζ_2 also bounded.*

Proof. The following LFC is proposed:

$$V_{\zeta_2} = \frac{1}{2}\zeta_2^2. \tag{A14}$$

Because the drag coefficients depend on the speed v and the dynamic equation is expressed by (10), a transformation to the form is made:

$$\dot{\zeta}_2 = \mathbb{N}_2^{-1}(-mz_g qr - m_{11} ur - d_{22} v - d_{25} r + f_v). \tag{A15}$$

Calculating the time derivative of (A14), one obtains

$$\dot{V}_{\zeta_2} = \zeta_2 \dot{\zeta}_2 = \zeta_2 \mathbb{N}_2^{-1}(-mz_g qr - m_{11} ur - d_{22} v - d_{25} r + f_v). \tag{A16}$$

Recalling ζ_2 (8), one can write

$$\dot{V}_{\zeta_2} = \mathbb{N}_2^{-1}(v - \hat{Y}_{25} r)(-mz_g qr - m_{11} ur - d_{22} v - d_{25} r + f_v). \tag{A17}$$

Defining $A_1 = \hat{Y}_{25} r$, $A_2 = -mz_g qr - m_{11} ur - d_{25} r + f_v$, one obtains

$$\dot{V}_{\zeta_2} = \mathbb{N}_2^{-1}(v - A_1)(A_2 - d_{22} v). \tag{A18}$$

To guarantee $\dot{V}_{\zeta_2} < 0$, four cases must be considered (recall that $\mathbb{N}_2 > 0$):

(1) $v < A_1 < 0$, $(A_2 - d_{22} v) > 0$, and $(v - A_1) < 0$,
(2) $A_1 < v < 0$, $(A_2 - d_{22} v) < 0$, and $(v - A_1) > 0$,
(3) $v > A_1 > 0$, $(A_2 - d_{22} v) < 0$, and $(v - A_1) > 0$,
(4) $0 < v < A_1$, $(A_2 - d_{22} v) > 0$, and $(v - A_1) < 0$. (A19)

Inserting values of d_{22}, d_{25}, as shown in Appendix A, and taking into account (A18), the fact that u, q, r are all controlled and limited, and also that function f_v is limited, it can be written that

$$(1), \ (2) \quad -v_{max} \leq v < \frac{Y_v - \sqrt{\Delta_1}}{2Y_{|v|v}}, \quad \text{and} \quad v < A_1, \tag{A20}$$

$$(3), \ (4) \quad v_{max} \geq v > \frac{-Y_v + \sqrt{\Delta_2}}{2Y_{|v|v}}, \quad \text{and} \quad v > A_1, \tag{A21}$$

where $\Delta_1 = Y_v^2 - 4Y_{|v|v}A_2$ and $\Delta_2 = Y_v^2 + 4Y_{|v|v}A_2$. Hence, it is clear that v decreases and hence it is bounded. And since $\zeta_2 = v - \hat{Y}_{25}r$, it can be deduced that ζ_2 is also bounded. $\square$

Lemma A2. *Assuming a limited disturbance function f_w, it is possible to limit the speed of w, which makes the rate of ζ_3 also bounded.*

Proof. The proposed LFC has the form

$$V_{\zeta_3} = \frac{1}{2}\zeta_3^2. \tag{A22}$$

Recalling (11) (with $\tau_w = 0$), one has

$$\dot{\zeta}_3 = \mathbb{N}_3^{-1}(m_{14}q^2 + m_{11}uq - d_{33}w - d_{34}q + f_w). \tag{A23}$$

Calculating the derivative of (A22) with respect to time leads to

$$\dot{V}_{\zeta_3} = \zeta_3\dot{\zeta}_3 = \zeta_3\mathbb{N}_3^{-1}(m_{14}q^2 + m_{11}uq - d_{33}w - d_{34}q + f_w). \tag{A24}$$

Since ζ_3 (8), thus

$$\dot{V}_{\zeta_3} = \mathbb{N}_3^{-1}(w - \hat{Y}_{34}q)(m_{14}q^2 + m_{11}uq - d_{33}w - d_{34}q + f_w). \tag{A25}$$

Denoting now $A_3 = \hat{Y}_{34}q$, $A_4 = m_{14}q^2 + m_{11}uq - d_{34}q + f_w$, one obtains

$$\dot{V}_{\zeta_3} = \mathbb{N}_3^{-1}(w - A_3)(A_4 - d_{33}w). \tag{A26}$$

To guarantee $\dot{V}_{\zeta_3} < 0$, four cases must be considered (recall that $\mathbb{N}_3 > 0$):

$$\begin{aligned}
&(1) \quad w < A_3 < 0, \quad (A_4 - d_{33}w) > 0, \quad \text{and} \quad (w - A_3) < 0,\\
&(2) \quad A_3 < w < 0, \quad (A_4 - d_{33}w) < 0, \quad \text{and} \quad (w - A_3) > 0,\\
&(3) \quad w > A_3 > 0, \quad (A_4 - d_{33}w) < 0, \quad \text{and} \quad (w - A_3) > 0,\\
&(4) \quad 0 < w < A_3, \quad (A_4 - d_{33}w) > 0, \quad \text{and} \quad (w - A_3) < 0.
\end{aligned} \tag{A27}$$

Taking into account (A26), the fact that u, q, r can all be controlled and limited, and that the function f_w is limited, one obtains

$$(1),\ (2) \quad -w_{max} \le w < \frac{Z_w - \sqrt{\Delta_3}}{2Z_{|w|w}}, \quad \text{and} \quad w < A_3, \tag{A28}$$

$$(3),\ (4) \quad w_{max} \ge w > \frac{-Z_w + \sqrt{\Delta_2}}{2Z_{|w|w}}, \quad \text{and} \quad w > A_3, \tag{A29}$$

where $\Delta_3 = Z_w^2 - 4Z_{|w|w}A_4$ and $\Delta_4 = Z_w^2 + 4Z_{|w|w}A_4$. Hence, it is clear that w is decreasing and therefore bounded. And since $\zeta_3 = w - \hat{Y}_{34}q$, it can be deduced that ζ_3 is also bounded. $\square$

Since the desired trajectory u_d is planned, and therefore limited, while the velocities u, w are due to constraints on the values generated by the thrusters, the errors y_e, z_e are also limited. Recall now Young's inequality $ab \le \frac{\epsilon^2}{2}|a|^2 + \frac{1}{2\epsilon^2}|b|^2$ for $(a, b) \in \mathcal{R}$, and ϵ is a positive number [38]. Using this inequality, one obtains $|vy_e| \le \frac{\epsilon^2}{2}|v|^2 + \frac{1}{2\epsilon^2}|y_e|^2$, $|z_ew| \le \frac{\epsilon^2}{2}|z_e|^2 + \frac{1}{2\epsilon^2}|w|^2$, and $2|z_eu_d| \le \epsilon^2|z_e|^2 + \frac{1}{\epsilon^2}|u_d|^2$. Denoting

$$\delta_1 = \frac{\epsilon^2}{2}|v|^2 + \frac{1}{2\epsilon^2}|y_e|^2 + \frac{\epsilon^2}{2}|z_e|^2 + \frac{1}{2\epsilon^2}|w|^2 + \epsilon^2|z_e|^2 + \frac{1}{\epsilon^2}|u_d|^2, \tag{A30}$$

the expression (A13) can be given in the following form:

$$\dot{V}_K \leq -k_x x_e^2 - k_\theta\, s^2\theta_e - k_\psi\, s^2\psi_e + \delta_1. \tag{A31}$$

The problem, however, is that the input desired velocities $\mu_{du}, \mu_{dq}, \mu_{dr}$ are some virtual inputs and this results in the fact that (A31) does not apply to vehicle dynamics. Hence, there is the need to design an additional dynamic control algorithm to guarantee that $\dot{V}_K \leq \delta_1$ where δ_1 means a constant.

Dynamic controller design. The dynamic controller's purpose is to guide the vehicle to the desired speeds using the signals τ_u, τ_q, and τ_r. The velocity errors are determined by

$$[u_e, q_e, r_e] = [u - u_d, q - q_d, r - r_d]^T. \tag{A32}$$

Taking into account (8), the IQVs are as follows:

$$\zeta_{1e} = \zeta_1 - \zeta_{1d} = u - u_d - \hat{Y}_{14}(q - q_d),$$
$$\zeta_{4e} = \zeta_4 - \zeta_{4d} = q - q_d, \ \ \zeta_{5e} = \zeta_5 - \zeta_{5d} = r - r_d. \tag{A33}$$

For the signal τ_u, the first integral sliding surface is taken:

$$S_{D1} = \zeta_{1e} + \lambda_1 \int_0^t \zeta_{1e}(\iota)d\iota, \tag{A34}$$

where $\lambda_1 > 0$ is a positive control gain. Making use of (9), one obtains the time derivative of S_{D1}, i.e., $\dot{S}_{D1} = \dot{\zeta}_{1e} + \lambda_1\zeta_{1e}$, where $\dot{\zeta}_{1e} = \dot{\zeta}_1 - \dot{\zeta}_{1d} = \dot{u} - \dot{u}_d - \hat{Y}_{14}(\dot{q} - \dot{q}_d)$:

$$\dot{S}_{D1} = \mathbb{N}_1^{-1}\big(F_1(\zeta) - \mathbb{N}_1\dot{\zeta}_{1d} + \mathbb{N}_1\lambda_1\zeta_{1e} + \tau_u + f_u\big). \tag{A35}$$

Control input τ_u. To guarantee that the error converges to zero along the sliding surface S_{D1}, the control input is designed as follows:

$$\tau_u = -\hat{F}_1(\zeta) + \hat{\mathbb{N}}_1\dot{\zeta}_{1d} - \hat{\mathbb{N}}_1\lambda_1\zeta_{1e} - \hat{f}_u - \Pi_1\text{sgn}(S_{D1}). \tag{A36}$$

The final term, according to Assumption 4, refers to the perturbation reduction in parameters, and $\hat{f}_u$ denotes the evaluated value of the external disturbance f_u. Next, the following LFC is considered:

$$V_{D1} = \frac{1}{2}\mathbb{N}_1 S_{D1}^2 + \frac{1}{2}\beta_1\tilde{f}_u^2, \tag{A37}$$

where $\tilde{f}_u = f_u - \hat{f}_u$ means the estimated disturbance force error and $\beta_1 > 0$ is a fixed control parameter. Calculating the time derivative of V_{D1} and applying (A35)–(A36) yields the following:

$$\dot{V}_{D1} = \mathbb{N}_1 S_{D1}\dot{S}_{D1} + \beta_1\tilde{f}_u\dot{\tilde{f}}_u = S_{D1}\big(F_1(\zeta) - \hat{F}_1(\zeta) + (\hat{\mathbb{N}}_1 - \mathbb{N}_1)\dot{\zeta}_{1d} + \lambda_1(\mathbb{N}_1 - \hat{\mathbb{N}}_1)\zeta_{1e}$$
$$-\Pi_1\text{sgn}(S_{D1})\big) + \tilde{f}_u S_{D1} + \beta_1\tilde{f}_u\dot{\tilde{f}}_u, \tag{A38}$$

where

$$F_1(\zeta) - \hat{F}_1(\zeta) = (m_{22} - \hat{m}_{22})vr + (\hat{m}_{33} - m_{33})wq + (\hat{m}_{34} - m_{34})q^2 + (m_{25} - \hat{m}_{25})r^2$$
$$+(\hat{d}_{11} - d_{11})u + (\hat{d}_{14} - d_{14})q. \tag{A39}$$

Referring to Assumption 2, the gain term Π_1 of the form

$$\Pi_1 = \tilde{m}_{22}|vr| + \tilde{m}_{33}|wq| + \tilde{m}_{34}|q^2| + \tilde{m}_{25}|r^2| + \tilde{d}_{11}|u| + \tilde{d}_{14}|q|$$
$$+\tilde{N}_1|\dot{\zeta}_{1d}| + \lambda_1\tilde{N}_1|\zeta_{1e}| + \rho_1, \tag{A40}$$

is applied. Using Assumption 3 (if uncertainties $\dot{f}_u$ are close to zero or $\dot{f}_u \neq 0$ are arbitrarily large and rapidly changing in time), the time derivative of (A38) can be written as

$$
\begin{aligned}
\dot{V}_{D1} = \mathbb{N}_1 S_{D1} \dot{S}_{D1} + \beta_1 \tilde{f}_u \dot{\tilde{f}}_u &\leq -\rho_1 |S_{D1}| + \tilde{f}_u S_{D1} + \beta_1 \tilde{f}_u \dot{\tilde{f}}_u \\
&= -\rho_1 |S_{D1}| + \tilde{f}_u S_{D1} + \beta_1 \tilde{f}_u (\dot{f}_u - \dot{\hat{f}}_u).
\end{aligned}
\tag{A41}
$$

By choosing the adaptation component of $\dot{\hat{f}}_u = \beta_1^{-1} S_{D1}$, one has

$$
\dot{V}_{D1} \leq -\rho_1 |S_{D1}| + \beta_1 \tilde{f}_u \dot{f}_u \leq -\rho_1 |S_{D1}| + \epsilon_1.
\tag{A42}
$$

Thus, one obtains $\dot{V}_{D1} = \epsilon_1$ provided that ζ_{1e} tends to zero along the sliding surface S_{D1}. However, $\zeta_{1e} = u_e - \hat{Y}_{14} q_e$, so $u_e = \hat{Y}_{14} q_e$. Therefore, to ensure that u_e converges to zero, it is also necessary to ensure that q_e goes to zero. This will be demonstrated later for S_{D2}.

For the bounded signal $\dot{f}_u$ (Assumption 3) and a well-designed controller, there exists a positive scalar $\epsilon_1 \geq |\beta_1 \tilde{f}_u \dot{f}_u|$. The condition $|\beta_1 \tilde{f}_u \dot{f}_u| < \rho_1 |S_{D1}|$ must be fulfilled to guarantee uniformly ultimate boundedness. This problem was considered in [37,45]. The second integral sliding surface is assumed to be

$$
S_{D2} = \zeta_{4e} + \lambda_2 \int_0^t \zeta_{4e}(\iota) d\iota,
\tag{A43}
$$

where $\lambda_2 > 0$ is a control parameter. Using Equation (12) one differentiates with respect to time S_{D2}, obtaining $\dot{S}_{D2} = \dot{\zeta}_{4e} + \lambda_2 \zeta_{4e}$ (where $\dot{\zeta}_{4e} = \dot{\zeta}_4 - \dot{\zeta}_{4d}$):

$$
\dot{S}_{D2} = \mathbb{N}_4^{-1} \big(F_4(\zeta) - \mathbb{N}_4 \dot{\zeta}_{4d} + \mathbb{N}_4 \lambda_2 \zeta_{3e} + \tau_{\zeta_4} + f_{\zeta_4} \big).
\tag{A44}
$$

Control input τ_{ζ_4}. The following input control signal τ_{ζ_4} is proposed:

$$
\tau_{\zeta_4} = -\hat{F}_4(\zeta) + \hat{\mathbb{N}}_4 \dot{\zeta}_{4d} - \hat{\mathbb{N}}_4 \lambda_2 \zeta_{4e} - \hat{f}_{\zeta_4} - \Pi_2 \mathrm{sgn}(S_{D2}),
\tag{A45}
$$

where the final component follows from Assumption 4 and is related to the function of the perturbation parameters and $\hat{f}_{\zeta_4}$ denotes the external disturbance force f_{ζ_4} estimated value.

Next, the following LFC is considered:

$$
V_{D2} = \frac{1}{2} \mathbb{N}_4 S_{D2}^2 + \frac{1}{2} \beta_2 \tilde{f}_{\zeta_4}^2,
\tag{A46}
$$

where $\tilde{f}_{\zeta_4} = f_{\zeta_4} - \hat{f}_{\zeta_4}$ is the disturbance force estimated error and $\beta_2 > 0$ is a selected constant. By differentiating V_{D2} with respect to time and using (A44)–(A45), one obtains

$$
\begin{aligned}
\dot{V}_{D2} = \mathbb{N}_4 S_{D2} \dot{S}_{D2} + \beta_2 \tilde{f}_{\zeta_4} \dot{\tilde{f}}_{\zeta_4} = S_{D2} \big(F_4(\zeta) - \hat{F}_4(\zeta) + (\hat{\mathbb{N}}_4 - \mathbb{N}_4) \dot{\zeta}_{4d} + \lambda_2 (\mathbb{N}_4 - \hat{\mathbb{N}}_4) \zeta_{4e} \\
- \Pi_2 \mathrm{sgn}(S_{D2}) \big) + \tilde{f}_{\zeta_4} S_{D2} + \beta_2 \tilde{f}_{\zeta_4} \dot{\tilde{f}}_{\zeta_4},
\end{aligned}
\tag{A47}
$$

where

$$
F_4(\zeta) - \hat{F}_4(\zeta) = \hat{Y}_{14} \big(F_1(\zeta) - \hat{F}_1(\zeta) \big) + \hat{Y}_{34} \big(F_3(\zeta) - \hat{F}_3(\zeta) \big) + F_{41}(\zeta) - \hat{F}_{41}(\zeta),
\tag{A48}
$$

with

$$
F_3(\zeta) - \hat{F}_3(\zeta) = (m_{11} - \hat{m}_{11}) uq + (m_{14} - \hat{m}_{14}) q^2 + (\hat{d}_{33} - d_{33}) w + (\hat{d}_{34} - d_{34}) q,
\tag{A49}
$$

$$
\begin{aligned}
F_{41}(\zeta) - \hat{F}_{41}(\zeta) = (m - \hat{m}) z_g vr + \big((m_{33} - \hat{m}_{33}) - (m_{11} - \hat{m}_{11}) \big) uw + (m_{34} - \hat{m}_{34}) uq \\
+ (\hat{m}_{14} - m_{14}) wq + (\hat{d}_{41} - d_{41}) u + (\hat{d}_{43} - d_{43}) w + (\hat{d}_{44} - d_{44}) q + (\hat{g}_4 - g_4).
\end{aligned}
\tag{A50}
$$

The quantity $F_1(\zeta) - \hat{F}_1(\zeta)$ is defined by (A39).

In order to provide stability of the control system when there is a perturbation of the parameters and recalling Assumption 2, the following gain function is proposed:

$$\Pi_2 = B_1|\hat{Y}_{14}| + B_2|\hat{Y}_{34}| + B_3 + \tilde{\mathbb{N}}_4|\dot{\zeta}_{4d}| + \lambda_3\tilde{\mathbb{N}}_4|\zeta_{4e}| + \rho_2, \tag{A51}$$

where

$$B_1 = \tilde{m}_{22}|vr| + \tilde{m}_{33}|wq| + \tilde{m}_{34}|q^2| + \tilde{m}_{25}|r^2| + \tilde{d}_{11}|u| + \tilde{d}_{14}|q|,$$
$$B_2 = \tilde{m}_{11}|uq| + \tilde{m}_{14}|q^2| + \tilde{d}_{33}|w| + \tilde{d}_{34}|q|,$$
$$B_3 = \tilde{m}z_g|vr| + (\tilde{m}_{33} - \tilde{m}_{11})|uw| + \tilde{m}_{34}|uq| + \tilde{m}_{14}|wq| + \tilde{d}_{41}|u| + \tilde{d}_{43}|w| + \tilde{d}_{44}|q|$$
$$\quad + \tilde{W}|z_g s\theta + x_g c\theta|.$$

Taking into account Assumption 3 and $\dot{f}_{\zeta_4}$ close to zero or $\dot{f}_{\zeta_4} \neq 0$ (it follows that at least one of the signals $\dot{f}_u$, $\dot{f}_w$, and $\dot{f}_q$ is non-zero), the derivative $\dot{V}_{D2}$ (A47) may be written in the form

$$\dot{V}_{D2} = \mathbb{N}_4 S_{D2}\dot{S}_{D2} + \beta_2 \tilde{f}_{\zeta_4}\dot{\tilde{f}}_{\zeta_4} \leq -\rho_2|S_{D2}| + \tilde{f}_{\zeta_4}S_{D2} + \beta_2\tilde{f}_{\zeta_4}(\dot{f}_{\zeta_4} - \dot{\hat{f}}_{\zeta_4}). \tag{A52}$$

The adaptive term is assumed as $\dot{\hat{f}}_{\zeta_4} = \beta_2^{-1}S_{D2}$. Then, one obtains

$$\dot{V}_{D2} \leq -\rho_2|S_{D2}| + \beta_2\tilde{f}_{\zeta_4}\dot{f}_{\zeta_4} \leq -\rho_2|S_{D2}| + \epsilon_2, \tag{A53}$$

where $\epsilon_2 \geq |\beta_2\tilde{f}_{\zeta_4}\dot{f}_{\zeta_4}|$ is a positive number if the control algorithm is well designed. Inequality $|\beta_2\tilde{f}_{\zeta_4}\dot{f}_{\zeta_4}| < \rho_2|S_{D2}|$ must be satisfied to guarantee uniformly ultimate boundedness.

If the assumption that ζ_{4e} goes to zero along the sliding surface S_{D2} is met, then $\dot{V}_{D2} = \epsilon_2$. Because $\zeta_{4e} = q_e$, q_e converges to zero. It follows that if a signal τ_{ζ_4} (A45) is used, the velocity q_e will converge to zero. Considering (A34) and (A42), it can be deduced that if q_e converges to zero, u_e also tends to zero.

The third integral sliding surface is defined as

$$S_{D3} = \zeta_{5e} + \lambda_3 \int_0^t \zeta_{5e}(\iota)d\iota, \tag{A54}$$

where $\lambda_3 > 0$ is a constant gain. Taking (13) into account, the time derivative of (A54) is of the form $\dot{S}_{D3} = \dot{\zeta}_{5e} + \lambda_3\zeta_{5e}$ (where $\dot{\zeta}_{5e} = \dot{\zeta}_5 - \dot{\zeta}_{5d}$):

$$\dot{S}_{D3} = \mathbb{N}_5^{-1}(F_5\zeta) - \mathbb{N}_5\dot{\zeta}_{5d} + \mathbb{N}_5\lambda_3\zeta_{5e} + \tau_r + f_{\zeta_5}). \tag{A55}$$

Control input τ_r. The yaw input τ_r is assumed as follows:

$$\tau_r = -\hat{F}_5(\zeta) + \hat{\mathbb{N}}_5\dot{\zeta}_{5d} - \hat{\mathbb{N}}_5\lambda_3\zeta_{5e} - \hat{f}_{\zeta_5} - \Pi_3\text{sgn}(S_{D3}), \tag{A56}$$

where the final component resulting from Assumption 4 refers to the function of uncertain parameters. Moreover, $\hat{f}_{\zeta_5}$ means the estimated value of external disturbance f_{ζ_5}.

The LFC is proposed in the following form:

$$V_{D3} = \frac{1}{2}\mathbb{N}_5 S_{D3}^2 + \frac{1}{2}\beta_3\tilde{f}_{\zeta_5}^2, \tag{A57}$$

where $\tilde{f}_{\zeta_5} = f_{\zeta_5} - \hat{f}_{\zeta_5}$ means the disturbance force estimated error while $\beta_3 > 0$ is a constant gain. Determining the derivative V_{D3} with respect to time and applying (A55)–(A56), one obtains

$$\dot{V}_{D3} = \mathbb{N}_5 S_{D3}\dot{S}_{D3} + \beta_3 \tilde{f}_{\zeta_5}\dot{\tilde{f}}_{\zeta_5} = S_{D3}\big(F_5(\zeta) - \hat{F}_5(\zeta) + (\hat{\mathbb{N}}_5 - \mathbb{N}_5)\dot{\zeta}_{5d} + \lambda_3(\mathbb{N}_5 - \hat{\mathbb{N}}_5)\zeta_{5e}$$
$$-\Pi_3 \mathrm{sgn}(S_{D3})\big) + \tilde{f}_{\zeta_5}S_{D3} + \beta_3 \tilde{f}_{\zeta_5}\dot{\tilde{f}}_{\zeta_5}, \tag{A58}$$

where

$$F_5(\zeta) - \hat{F}_5(\zeta) = \hat{Y}_{25}\big(F_2(\zeta) - \hat{F}_2(\zeta)\big) + F_{51}(\zeta) - \hat{F}_{51}(\zeta), \tag{A59}$$

with

$$F_2(\zeta) - \hat{F}_2(\zeta) = (\hat{m} - m)z_g qr + (\hat{m}_{11} - m_{11})ur + (\hat{d}_{22} - d_{22})v + (\hat{d}_{25} - d_{25})r,$$
$$F_{51}(\zeta) - \hat{F}_{51}(\zeta) = (\hat{m}_{25} - m_{25})ur + \big((m_{11} - \hat{m}_{11}) - (m_{22} - \hat{m}_{22})\big)uv$$
$$+(\hat{d}_{52} - d_{52})v + (\hat{d}_{55} - d_{55})r. \tag{A60}$$

In order to guarantee the control system's stability under the parameter perturbations and taking into account Assumption 2, the proposed gain function is

$$\Pi_3 = B_4|\hat{Y}_{25}| + B_5 + \tilde{\mathbb{N}}_5|\dot{\zeta}_{5d}| + \lambda_4 \tilde{\mathbb{N}}_5|\zeta_{5e}| + \rho_3, \tag{A61}$$

where

$$B_4 = \tilde{m}z_g|qr| + \tilde{m}_{11}|ur| + \tilde{d}_{22}|v| + \tilde{d}_{25}|r|,$$
$$B_5 = \tilde{m}_{25}|ur| + (\tilde{m}_{11} - \tilde{m}_{22})|uv| + \tilde{d}_{52}|v| + \tilde{d}_{55}|r|. \tag{A62}$$

Recalling Assumption 3 and $\dot{f}_{\zeta_5}$ close to zero or $\dot{f}_{\zeta_5} \neq 0$ (which means that at least $\dot{f}_v$ and $\dot{f}_r$ are different from zero), the function $\dot{V}_{D4}$ (A58) can be written in the following form:

$$\dot{V}_{D3} = \mathbb{N}_5 S_{D3}\dot{S}_{D3} + \beta_3 \tilde{f}_{\zeta_5}\dot{\tilde{f}}_{\zeta_5} \leq -\rho_3|S_{D3}| + \tilde{f}_{\zeta_5}S_{D3} + \beta_3 \tilde{f}_{\zeta_5}(\dot{f}_{\zeta_5} - \dot{\hat{f}}_{\zeta_5}). \tag{A63}$$

The adaptive term is assumed as $\dot{\hat{f}}_{\zeta_5} = \beta_3^{-1}S_{D3}$. Thus, one obtains

$$\dot{V}_{D3} \leq -\rho_3|S_{D3}| + \beta_3 \tilde{f}_{\zeta_5}\dot{f}_{\zeta_5} \leq -\rho_3|S_{D3}| + \epsilon_3, \tag{A64}$$

where $\epsilon_3 \geq |\beta_3 \tilde{f}_{\zeta_5}\dot{\hat{f}}_{\zeta_5}|$ is a positive scalar that can be found if $\dot{f}_r$ (Assumption 3) is limited and the controller is well designed. Moreover, the condition $|\beta_3 \tilde{f}_{\zeta_5}\dot{\hat{f}}_{\zeta_5}| < \rho_3|S_{D3}|$ must be fulfilled to guarantee uniformly ultimate boundedness.

Hence, if ζ_{5e} tends to zero along the sliding surface S_{D3}, then $\dot{V}_{D3} = \epsilon_3$. Because $\zeta_{5e} = r_e$, r_e tends to zero. Consequently, if τ_r (A56) is applied, the velocity error r_e will converge to zero.

Therefore, for functions $\dot{f}_u \neq 0$, $\dot{f}_v \neq 0$, $\dot{f}_w \neq 0$, $\dot{f}_q \neq 0$ or $\dot{f}_r \neq 0$ or when $\dot{f}_u, \dot{f}_v, \dot{f}_w, \dot{f}_q, \dot{f}_r$ are approximately zero, one obtains

$$\dot{V}_D = \dot{V}_{D1} + \dot{V}_{D2} + \dot{V}_{D3} \leq -\rho_1|S_{D1}| - \rho_2|S_{D2}| - \rho_3|S_{D3}| + \epsilon_4, \tag{A65}$$

where $\epsilon_4 = \epsilon_1 + \epsilon_2 + \epsilon_3$ is a positive scalar. Summarizing, in the considered case, only uniformly ultimate boundedness can be guaranteed.

Stability analysis. The results are compiled and summarized in the proof shown below.

Proof of Theorem 1. Consider the vehicle and working conditions according to Assumptions $1 \div 5$. For the stability analysis, the following LFC is assumed:

$$V_F = V_K + V_{D1} + V_{D2} + V_{D3} = \frac{1}{2}x_e^2 + \frac{1}{2}y_e^2 + \frac{1}{2}z_e^2 + (1 - c\theta_e) + (1 - c\psi_e)$$
$$+ \frac{1}{2}\mathbb{N}_1 S_{D1}^2 + \frac{1}{2}\beta_1 \tilde{f}_u^2 + \frac{1}{2}\mathbb{N}_4 S_{D2}^2 + \frac{1}{2}\beta_2 \tilde{f}_{\zeta_4}^2 + \frac{1}{2}\mathbb{N}_5 S_{D3}^2 + \frac{1}{2}\beta_3 \tilde{f}_{\zeta_5}^2. \tag{A66}$$

The use of a kinematic controller alone does not ensure the convergence of linear and angular position errors. For this reason, a dynamic controller is designed to guide the vehicle to the desired trajectory and provide the uniform ultimate boundedness. The results achieved can be summarized in the following expression:

$$\dot{V}_F = \dot{V}_K + \dot{V}_{D1} + \dot{V}_{D2} + \dot{V}_{D3} = -k_x x_e^2 - k_\theta s^2\theta_e - k_\psi s^2\psi_e + vy_e$$
$$+ z_e\big(w + u_d(1 - c\psi_e)c\theta s\theta_d\big) + \mathbb{N}_1 S_{D1}\dot{S}_{D1} + \beta_1 \tilde{f}_u \dot{\tilde{f}}_u + \mathbb{N}_4 S_{D2}\dot{S}_{D2} + \beta_2 \tilde{f}_{\zeta_4}\dot{\tilde{f}}_{\zeta_4}$$
$$+ \mathbb{N}_5 S_{D3}\dot{S}_{D3} + \beta_3 \tilde{f}_{\zeta_5}\dot{\tilde{f}}_{\zeta_5} \leq -k_x x_e^2 - k_\theta s^2\theta_e - k_\psi s^2\psi_e$$
$$- \rho_1|S_{D1}| - \rho_2|S_{D2}| - \rho_3|S_{D3}| + \delta_1 + \epsilon_4. \tag{A67}$$

Denoting

$$\mathcal{Z} = k_x x_e^2 + k_\theta s^2\theta_e + k_\psi s^2\psi_e + \rho_1|S_{D1}| + \rho_2|S_{D2}| + \rho_3|S_{D3}| - \delta_1, \tag{A68}$$

it can be seen that $\mathcal{Z} \geq 0$ if

$$k_x x_e^2 + k_\theta s^2\theta_e + k_\psi s^2\psi_e + \rho_1|S_{D1}| + \rho_2|S_{D2}| + \rho_3|S_{D3}| \geq \delta_1. \tag{A69}$$

The signals included in δ_1, i.e., v, y_e, v, z_e, and u_d, are limited. This means that by appropriately selecting ϵ and tuning the parameters k_x, k_θ, k_ψ, ρ_1, ρ_2, and ρ_3, unwanted elements may be decreased in value. Through the appropriate selection of design gains, the proposed τ_u (A36), τ_{ζ_4} (A45), and τ_r (A56) control signals ensure that the desired trajectory is traced in three-dimensional space when parameter perturbations and external disturbances occur. Therefore, it can be written that

$$\dot{V}_F \leq -\mathcal{Z} + \epsilon_4. \tag{A70}$$

This implies that all tracking errors in the closed-loop system converge to a small neighborhood of the origin and are hence uniformly ultimately bounded. In summary, the results obtained end this proof. □

References

1. Do, K.D.; Pan, J. *Control of Ships and Underwater Vehicles*; Springer: London, UK, 2009.
2. Fossen, T.I. *Guidance and Control of Ocean Vehicles*; John Wiley and Sons: Chichester, UK, 1994.
3. Aguiar, A.P.; Hespanha, J.P. Trajectory-Tracking and Path-Following of Underactuated Autonomous Vehicles With Parametric Modeling Uncertainty. *IEEE Trans. Autom. Control.* **2007**, *52*, 1362–1379.
4. Kim, J.H.; Yoo, S.J. Adaptive Event-Triggered Control Strategy for Ensuring Predefined Three-Dimensional Tracking Performance of Uncertain Nonlinear Underactuated Underwater Vehicles. *Mathematics* **2021**, *9*, 137. https://doi.org/10.3390/math9020137.
5. Hu, Y.; Li, B.; Jiang, B.; Han, J.; Wen, C.-Y. Disturbance Observer-Based Model Predictive Control for an Unmanned Underwater Vehicle. *J. Mar. Sci. Eng.* **2024**, *12*, 94. https://doi.org/10.3390/jmse12010094.
6. Duan, K.; Fong, S.; Chen, C.L.P. Fuzzy observer-based tracking control of an underactuated underwater vehicle with linear velocity estimation. *IET Control. Theory Appl.* **2020**, *14*, 584–593.
7. Thanh, P.N.N.; Thuyen, N.A.; Anh, H.P.H. Adaptive fuzzy 3-D trajectory tracking control for autonomous underwater vehicle (AUV) using modified integral barrier lyapunov function. *Ocean Eng.* **2023**, *283*, 115027.
8. Fetzer, K.L.; Nersesov, S.; Ashrafiuon, H. Nonlinear control of three-dimensional underactuated vehicles. *Int. J. Robust Nonlinear Control.* **2020**, *30*, 1607–1621.
9. Fang, Y.; Huang, Z.; Pu, J.; Zhang, J. AUV position tracking and trajectory control based on fast-deployed deep reinforcement learning method. *Ocean Eng.* **2022**, *245*, 110452.

10. Xu, R.; Tang, G.; Xie, D.; Han, L.; Huang, H. Neural network for 3D trajectory tracking control of a CMG-actuated underwater vehicle with input saturation. *ISA Trans.* **2022**, *123*, 152–167.

11. Ferreira, C.Z.; Cardoso, R.; Meza, M.E.M.; Avila, J.P.J. Controlling tracking trajectory of a robotic vehicle for inspection of underwater structures. *Ocean Eng.* **2018**, *149*, 373–382.

12. Li, Y.; Wei, C.; Wu, Q.; Chen, P.; Jiang, Y.; Li, Y. Study of 3 dimension trajectory tracking of underactuated autonomous underwater vehicle. *Ocean Eng.* **2015**, *105*, 270–274.

13. Wang, Z.; Xiang, X.; Duan, Y.; Yang, S. Adversarial deep reinforcement learning based robust depth tracking control for underactuated autonomous underwater vehicle. *Eng. Appl. Artif. Intell.* **2024**, *130*, 107728.

14. Cao, J.; Sun, Y.; Zhang, G.; Jiao, W., Wang, X.; Liu, Z. Target tracking control of underactuated autonomous underwater vehicle based on adaptive nonsingular terminal sliding mode control. *Int. J. Adv. Robot. Syst.* **2020**, *17*, 1–13. https://doi.org/10.1177/1729881420919941.

15. Gong, H.; Er, M.J.; Liu, Y.; Ma, C. Three-dimensional optimal trajectory tracking control of underactuated AUVs with uncertain dynamics and input saturation. *Ocean Eng.* **2024**, *298*, 116757.

16. Li, J.; Du, J.; Chen, C.L.P. Command-Filtered Robust Adaptive NN Control With the Prescribed Performance for the 3-D Trajectory Tracking of Underactuated AUVs. *IEEE Trans. Neural Netw. Learn. Syst.* **2022**, *33*, 6545–6557.

17. Liu, J.; Du, J. Composite learning tracking control for underactuated autonomous underwater vehicle with unknown dynamics and disturbances in three-dimension space. *Appl. Ocean Res.* **2021**, *112*, 102686.

18. Xu, J.; Cui, Y.; Yan, Z.; Huang, F.; Du, X.; Wu, D. Event-triggered adaptive target tracking control for an underactuated autonomous underwater vehicle with actuator faults. *J. Frankl. Inst.* **2023**, *360*, 2867–2892.

19. Li, J.; Du, J.; Zhu, G.; Lewis, F.L. Simple adaptive trajectory tracking control of underactuated autonomous underwater vehicles under LOS range and angle constraints. *IET Control Theory Appl.* **2020**, *14*, 283–290.

20. Wu, Z.; Peng, H.; Hu, B.; Feng, X. Trajectory Tracking of a Novel Underactuated AUV via Nonsingular Integral Terminal Sliding Mode Control. *IEEE Access* **2021**, *9*, 103407–103418.

21. Che, G.; Hu, X. Optimal trajectory-tracking control for underactuated AUV with unknown disturbances via single critic network based adaptive dynamic programming. *J. Ambient Intell. Humaniz. Comput.* **2023**, *14*, 7265–7279.

22. Jiang, Y.; Guo, C.; Yu, H. Robust trajectory tracking control for an underactuated autonomous underwater vehicle based on bioinspired neurodynamics. *Int. J. Adv. Robot. Syst.* **2018**, *15*. https://doi.org/10.1177/1729881418806745.

23. Yan, Z.; Wang, M.; Xu, J. Integrated guidance and control strategy for homing of unmanned underwater vehicles. *J. Frankl. Inst.* **2019**, *356*, 3831–3848.

24. Zhou, J.; Ye, D.; Zhao, J.; He, D. Three-dimensional trajectory tracking for underactuated AUVs with bio-inspired velocity regulation. *Int. J. Nav. Archit. Ocean Eng.* **2018**, *10*, 282–293.

25. Xie, T.; Li, Y.; Jiang, Y.; An, L.; Wu H. Backstepping active disturbance rejection control for trajectory tracking of underactuated autonomous underwater vehicles with position error constraint. *Int. J. Adv. Robot. Syst.* **2020**, *17*. https://doi.org/10.1177/1729881420909633.

26. Yu, H.; Guo, C.; Yan, Z. Globally finite-time stable three-dimensional trajectory-tracking control of underactuated UUVs. *Ocean Eng.* **2019**, *189*, 106329.

27. Zhou, J.; Zhao, X.; Feng, Z.; Wu, D. Trajectory tracking sliding mode control for underactuated autonomous underwater vehicles with time delays. *Int. J. Adv. Robot. Syst.* **2020**, *17*. https://doi.org/10.1177/1729881420916276.

28. Li, Y.; He, J.; Shen, H.; Zhang, W.; Li, Y. Adaptive practical prescribed-time fault-tolerant control for autonomous underwater vehicles trajectory tracking. *Ocean Eng.* **2023**, *277*, 114263.

29. Cho, G.R.; Kang, H.; Kim, M.G.; Lee, M.J.; Li, J.H.; Kim, H.; Lee, H.; Lee, G. An Experimental Study on Trajectory Tracking Control of Torpedo-like AUVs Using Coupled Error Dynamics. *J. Mar. Sci. Eng.* **2023**, *11*, 1334. https://doi.org/10.3390/jmse11071334.

30. Wiig, M.S.; Pettersen, K.Y.; Krogstad, T.R. A 3D reactive collision avoidance algorithm for underactuated underwater vehicles. *J. Field Robot.* **2020**, *37*, 1094–1122.

31. Loduha, T.A.; Ravani, B. On First-Order Decoupling of Equations of Motion for Constrained Dynamical Systems. *Trans. ASME J. Appl. Mech.* **1995**, *62*, 216–222.

32. Herman, P. Application of nonlinear controller for dynamics evaluation of underwater vehicles. *Ocean Eng.* **2019**, *179*, 59–66.

33. Yu, H.; Guo, C.; Shen, Z.; Yan, Z. Output Feedback Spatial Trajectory Tracking Control of Underactuated Unmanned Undersea Vehicles. *IEEE Access* **2020**, *8*, 42924–42936.

34. Borhaug, E.; Pettersen, K.Y. Cross-track control for underactuated autonomous vehicles. In Proceedings of the 44th IEEE Conference on Decision and Control, Seville, Spain, 12–15 December 2005; pp. 602–608.

35. Qiao, L.; Zhang, W. Double-Loop Integral Terminal Sliding Mode Tracking Control for UUVs With Adaptive Dynamic Compensation of Uncertainties and Disturbances. *IEEE J. Ocean. Eng.* **2019**, *44*, 29–53.

36. Zhang, M.; Liu, X.; Yin, B.; Liu, W. Adaptive terminal sliding mode based thruster fault tolerant control for underwater vehicle in time-varying ocean currents. *J. Frankl. Inst.* **2015**, *352*, 4935–4961.

37. Soylu, S.; Buckham, B.J.; Podhorodeski, R.P. A chattering-free sliding-mode controller for underwater vehicles with fault-tolerant infinity-norm thrust allocation. *Ocean Eng.* **2008**, *35*, 1647–1659.

38. Do, K.D. Robust adaptive tracking control of underactuated ODINs under stochastic sea loads. *Robot. Auton. Syst.* **2015**, *72*, 152–163.

39. Mitchell, A.J.; McGookin, E.W.; Murray-Smith, D.J. Implementation of Sliding Mode Observer Based Reconfiguration in an Autonomous Underwater Vehicle. *Acta Polytech.* **2005**, *45*, 18–24.
40. Wang, Y.; Zhang, M.; Wilson, P.A.; Liu X. Adaptive neural network-based backstepping fault tolerant control for underwater vehicles with thruster fault. *Ocean Eng.* **2015**, *110*, 15–24.
41. Herman, P. Numerical Test of Several Controllers for Underactuated Underwater Vehicles. *Appl. Sci.* **2020**, *10*, 8292. https://doi.org/10.3390/app10228292.
42. Jiang, Y.; Guo, Ch.; Yu, H. Horizontal Trajectory Tracking Control for an Underactuated AUV Adopted Global Integral Sliding Mode Control. In Proceedings of 2018 Chinese Control And Decision Conference (CCDC), Shenyang, China, 9–11 June 2018; pp. 5786–5791.
43. Fierro, R.; Lewis, F.L. Control of a nonholonomic mobile robot: Backsteping kinematics into dynamics. In Proceedings of the 34th IEEE conference on Decision and Control, New Orleans Hilton Riverside, New Orleans, Louisiana 13–15 December 1995; pp. 3805–3810.
44. Herman, P. Robust trajectory tracking control scheme using transformed velocities for asymmetric underactuated marine vehicles. *Ocean Eng.* **2023** *285*, 115379.
45. Zeinali, M.; Notash, L. Adaptive sliding mode control with uncertainty estimator for robot manipulators. *Mech. Mach. Theory* **2010**, *45*, 80–90.